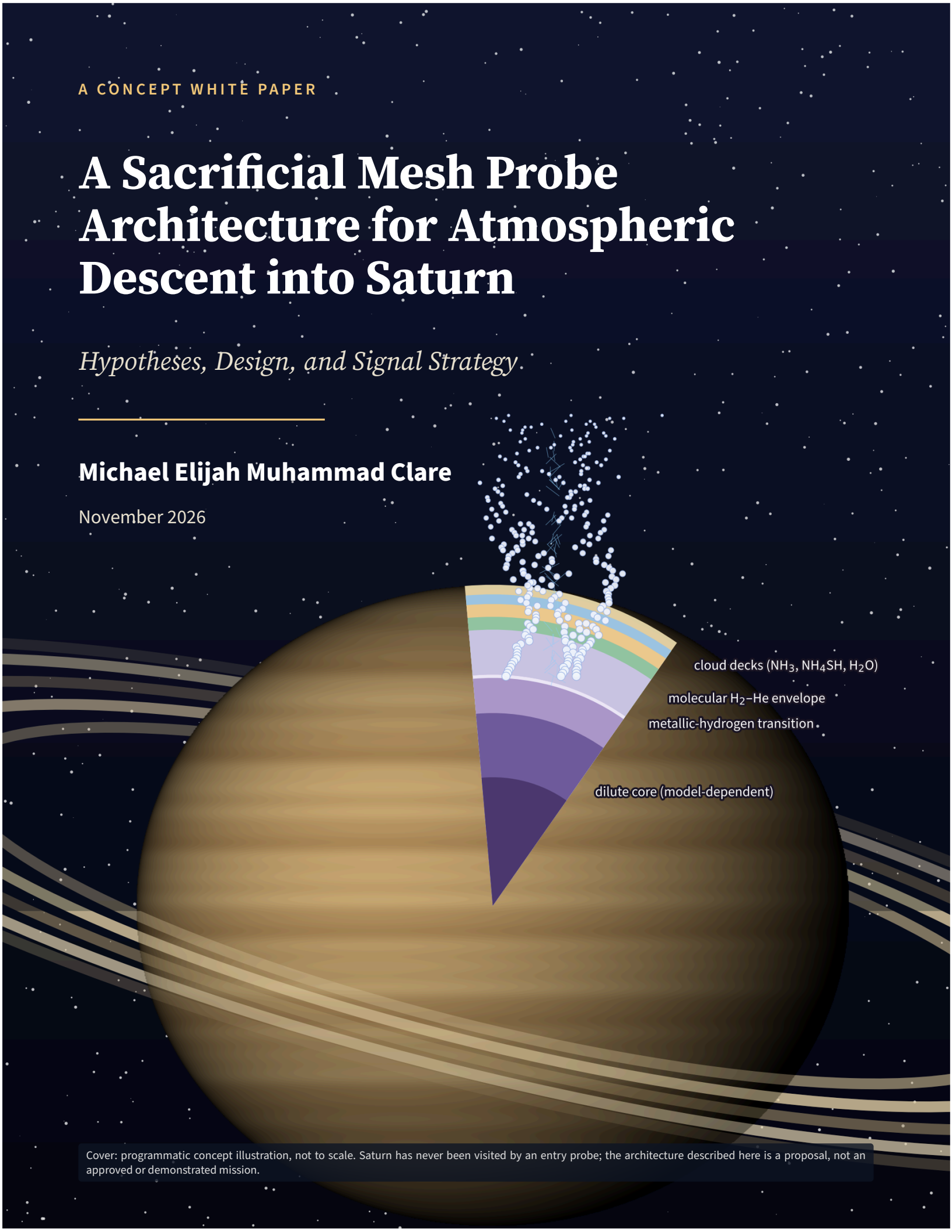
A CONCEPT WHITE PAPER

A Sacrificial Mesh Probe Architecture for Atmospheric Descent into Saturn

Hypotheses, Design, and Signal Strategy

Michael Elijah Muhammad Clare

November 2026



Cover: programmatic concept illustration, not to scale. Saturn has never been visited by an entry probe; the architecture described here is a proposal, not an approved or demonstrated mission.

A Sacrificial Mesh Probe Architecture for Atmospheric Descent into Saturn: Hypotheses, Design, and Signal Strategy

Michael Elijah Muhammad Clare
Independent Researcher, The Bahamas
November 2026

Author's Note

I am a software developer, not a trained scientist or physicist. The architecture in this paper (nested sacrificial shells, a swarm of golf-ball-sized nodes, a descending relay mesh, and an iterative loop between Saturn data and Earth laboratories) is my own idea, and I have tried to place it against the published science as carefully as I can. I offer it with humility and with genuine openness to correction. An outsider can sometimes see a problem from an angle the specialist community has not prioritised, and I think that perspective is worth more when it is put forward for scrutiny than when it is held back. Every hypothesis here is labelled as such, and I welcome specialists finding where it fails.

How to read this paper

Established science is stated with a citation. Proposed elements carry one of five labels: HYPOTHESIS (a conjecture to be tested), UNTESTED (no test data exist), INFERENCE (reasoned from cited physics but not shown in a source), ESTIMATE (a calculation in this paper with stated assumptions), and ORDER-OF-MAGNITUDE DESIGN ESTIMATE, NOT A DERIVED MISSION REQUIREMENT. Section 15 lists every correction, uncertainty, and partly verified citation; Appendix A gives the quantitative analysis.

Units and conversions used throughout

1 bar = 10^5 Pa = 0.98692 atm; 1 atm = 1.01325 bar = 101,325 Pa. For Saturn's cloud decks, bar and atm differ by about 1%, so "8–21 bar" is "≈8–21 atm". 1 kbar = 10^3 bar ≈ 987 atm. 1 GPa = 10 kbar = 10^4 bar ≈ 9,869 atm. 1 Mbar = 100 GPa = 10^6 bar ≈ 9.87 × 10^5 atm. 1 TPa = 1,000 GPa = 10 Mbar. Temperatures are in kelvin (0 °C = 273.15 K). Masses are sometimes in Earth masses ($M_\oplus$). Electrical conductivity σ is in S/m. 1 Ci = 3.7 × 10^{10} Bq by definition. "Saturn radius" R means the 1-bar equatorial radius, 60,268 km (Williams, n.d.).

Contents

1 Abstract . . . 5
2 Introduction and Motivation . . . 5
3 Background: Saturn's Atmosphere and Interior . . . 6
3.1 Troposphere and NH_3 clouds (≈1–2 bar; ≈1–2 atm; ≈0.1–0.2 MPa) . . . 7
3.2 NH_4SH clouds (≈2.5–5 bar; ≈2.5–4.9 atm) . . . 7
3.3 Water clouds (≈8–21 bar; ≈8–21 atm; ≈0.8–2.1 MPa) . . . 7
3.4 The molecular H_2–He envelope (≈20 bar to ≈1 Mbar; up to ≈10^6 atm) . . . 7
3.5 The metallic-hydrogen transition (≈0.8–2 Mbar; ≈80–200 GPa; ≈0.8–2 × 10^6 atm) . . . 7
3.6 The fuzzy (dilute) core (≈1–10 Mbar and deeper) . . . 7
4 Core Hypothesis: Nested Sacrificial Shells . . . 8
5 Golf-Ball Probe Design . . . 8
6 Mesh Network Bus Architecture . . . 9
7 Power . . . 11
8 Signal Strategy . . . 13
9 Material Science Frontier . . . 14
10 Enhancements . . . 16
11 Iterative Descent: The Closed Feedback Loop . . . 17
12 Limitations and Open Problems . . . 18
13 Conclusion . . . 19
14 Path to Funding and Next Steps . . . 19
15 Notes on Uncertainties and Factual Corrections . . . 20
15.1 Corrections to earlier informal estimates . . . 20
15.2 Uncertain or model-dependent values . . . 20
15.3 Calculations, extrapolations, and design labels . . . 21
15.4 Partly verified citations . . . 21
A Quantitative Analysis: Math, Materials, and Probability . . . 22
A.1 Node spacing and link range in a conducting medium . . . 22
A.2 Survival window and probability of completing an uplink . . . 23
A.3 Relay chain reliability . . . 24
A.4 Material stress on a golf-ball shell . . . 24
A.5 Power budget . . . 25
A.6 Atmospheric entry heating and survival fraction . . . 26
References . . . 27

List of Figures

Figure 1 Saturn's layered structure . . . 6
Figure 2 Exploded view of a concept node . . . 9
Figure 3 Mesh bus concept . . . 10
Figure 4 Waste-derived power path and capsule concept . . . 12
Figure 5 Signal comparison by band . . . 13
Figure 6 A high-pressure periodic table concept . . . 15
Figure 7 Laboratory analogues: DAC and laser ramp compression . . . 15
Figure 8 Concept of operations, orbiter to swarm . . . 17
Figure 9 Iterative descent: the closed feedback loop . . . 18

List of Tables

Table 1 Magnitude checks of informal estimates 8
Table 2 Candidate isotopes for node or dispenser power 12
Table 3 Link families compared 14
Table 4 Required MI transmit power versus gap and conductivity 23
Table 5 Survival windows and uplink-completion probabilities 24
Table 6 Relay chain reliability versus per-link failure probability 24
Table 7 Shell failure pressure by material 25
Table 8 Betavoltaic power and transmitter duty cycle 26
Table 9 Parametric entry-heating survival fraction for bare nodes 27

1 Abstract

Saturn has never been entered by an atmospheric probe. Everything known about its deep atmosphere and interior comes from remote sensing, the Voyager and Cassini missions, ring seismology, and laboratory and theoretical physics, and interior properties remain model-dependent (Iess et al., 2019; Mankovich and Fuller, 2021; Fortney et al., 2023). The only giant-planet entry probe flown, Galileo at Jupiter, returned data for about 58 minutes and measured the atmosphere to about 22 bar before its signal ended (Young, 1998; NASA, n.d.-b). This paper proposes, as a hypothesis for scrutiny, a different architecture: a large tranche (initially 10,000) of golf-ball-sized, sacrificial nodes, each built as nested shells sized to the pressure band it is meant to survive, released in sequence from a dispenser so that each node relays data to the node above it, forming a moving vertical mesh. I review Saturn's layered structure with pressures in atm, bar and GPa, and correct an earlier informal estimate (water clouds lie near 8–21 bar, not "thousands of atmospheres"). I compare candidate links: UHF/L-band in the upper, non-conducting troposphere; ELF/VLF or magnetic-induction links for the deepest, conducting layers; and optical links. I also assess power sources (rejecting Cs-137 and distinguishing purpose-made Pu-238 from spent-fuel plutonium), materials limits informed by diamond-anvil-cell and dynamic-compression experiments, and an order-of-magnitude node spacing of hundreds of metres to about 1 km. I then propose an iterative research loop in which Saturn data guide Earth-laboratory synthesis of the shell materials for the next probe generation, and outline realistic funding routes. A quantitative appendix works through link budgets, survival windows, chain reliability, shell stresses, power, and entry heating. Its most important result is negative: golf-ball magnetic-induction coils close only metre-to-tens-of-metres hops at milliwatt power, so the deep-link problem is the concept's critical open question. None of the architecture has been built or tested.

2 Introduction and Motivation

In situ measurements are the only way to obtain several key quantities for a giant planet: noble-gas and isotopic abundances, the deep water abundance, and the true vertical temperature profile beneath the clouds. The case for a Saturn probe has been made in detail by Mousis et al. (2014), who argue that a probe reaching at least 10 bar would substantially constrain models of Saturn's formation. A dedicated mission concept, Hera, was studied on that basis (Mousis et al., 2016). Galileo's probe showed both the value and the limits of a single, monolithic probe. Its entry site turned out to be an atypical, dry "5-µm hot spot", so it sampled one column that did not represent the planet's global water abundance (Young, 2003). Its link was also attenuated by ammonia absorption with depth (Folkner et al., 1998).

Saturn itself has hosted orbiters but no entry probe. Cassini ended its mission by diving into the planet on 15 September 2017. It was an orbiter destroyed on entry, not an instrumented descent probe (NASA, n.d.-a). Huygens, carried by Cassini, landed on Titan, not on Saturn.

The motivating idea is simple. Instead of one heavy probe that must survive as long as possible, release many small, cheap, deliberately sacrificial nodes in sequence. Each node operates only within the pressure band its shells can tolerate. The chain of nodes behaves like a moving relay ladder, carrying measurements from the deepest live node up to the dispenser and the orbiter. The approach trades individual survivability for statistical coverage, redundancy, and a relay path that is renewed continuously as old nodes are lost. HYPOTHESIS The central claim is that a relay chain of small sacrificial nodes could return useful data from deeper than any single probe of equal total mass. I could not find this analysed in the literature, and it is offered for testing.

Section 3 reviews the established structure of Saturn. Sections 4–7 describe the proposed shells, node, mesh bus, and power. Section 8 treats signal strategy, Section 9 the high-pressure materials frontier,

and Section 10 enhancements, including the spacing estimate. Section 11 proposes an iterative descent programme. Sections 12–14 cover limitations, conclusions, and funding, and Section 15 gives an explicit ledger of uncertainties and corrections. Appendix A contains the quantitative analysis.

3 Background: Saturn's Atmosphere and Interior

Saturn's equatorial radius at the 1-bar level is 60,268 km, its equatorial gravity is near 9 m/s^2 (mean about 11.2 m/s^2), the temperature near 1 bar is about 134 K, the density there is 0.19 kg/m^3, the scale height is about 59.5 km, and the mean molecular weight is 2.07 g/mol (Williams, n.d.). Interior-model papers adopt slightly different 1-bar temperatures (for example about 135 K or about 143 K), reflecting a later re-analysis of Voyager occultation data (Lindal et al., 1985; Militzer and Hubbard, 2023; Fortney et al., 2023). Pressure increases by roughly a factor of e every scale height near the cloud tops, so the cloud decks lie within the outer few hundred kilometres of a planet more than 60,000 km in radius. Figure 1 summarises the layers discussed below.

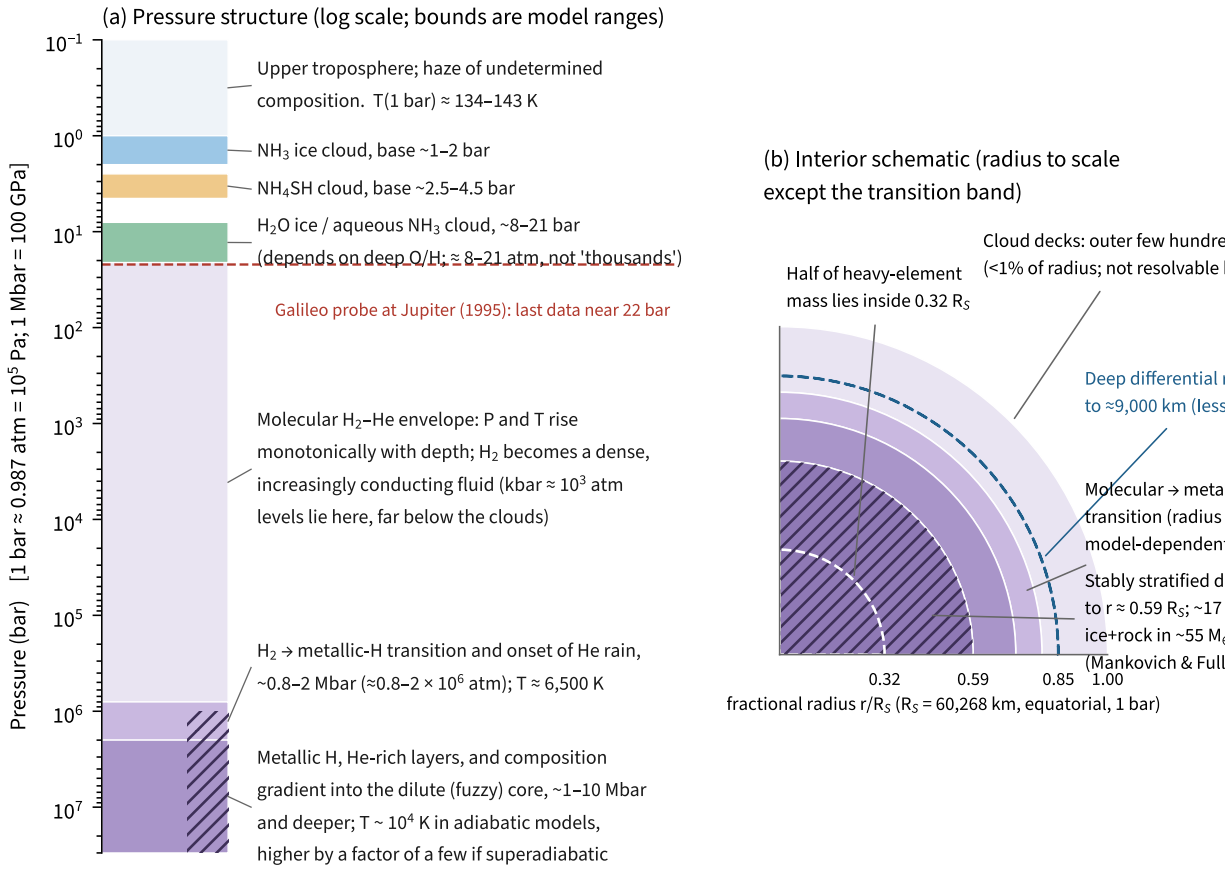


Figure 1: Saturn's layered structure. (a) Log-pressure column from 0.1 bar to beyond 10 Mbar with cloud decks, the molecular H_2–He envelope, the region where hydrogen becomes metallic and helium rain may begin, and the dilute core. Ranges are model-dependent and drawn from Del Genio et al. (2009), Mousis et al. (2014), Mankovich and Fuller (2021), Militzer and Hubbard (2023), and Fortney et al. (2023). The dashed red line marks the deepest Galileo measurement at Jupiter (≈22 bar), shown for scale only. (b) Schematic quarter-section (not to scale for the thin outer layers).

3.1 Troposphere and NH_3 clouds (≈1–2 bar; ≈1–2 atm; ≈0.1–0.2 MPa)

The uppermost cloud deck is ammonia ice. Equilibrium cloud models place its base at about 1 bar for solar abundances (Weidenschilling and Lewis, 1973; Del Genio et al., 2009) and at about 1.8 bar for a 5× solar enrichment (Mousis et al., 2014). Temperatures here are 130–150 K. This is the regime where existing entry-probe technology is mature.

3.2 NH_4SH clouds (≈2.5–5 bar; ≈2.5–4.9 atm)

Ammonia and hydrogen sulphide combine to form ammonium hydrosulphide. Models place this deck near 3–4 bar (Del Genio et al., 2009) or about 4 bar at 5× solar (Mousis et al., 2014). Cassini VIMS detected a deep cloud base at 2.5–4.5 bar, consistent with NH_4SH (Del Genio et al., 2009).

3.3 Water clouds (≈8–21 bar; ≈8–21 atm; ≈0.8–2.1 MPa)

The deepest condensation cloud is water ice and, lower down, an aqueous ammonia solution. Its base lies near 8–10 bar for solar O/H (Weidenschilling and Lewis, 1973; Del Genio et al., 2009) and moves to about 12.6–21 bar for enriched O/H, with about 20 bar for 5× solar (Mousis et al., 2014). **Correction:** an earlier informal version of this concept placed the deep water clouds at "thousands of atmospheres". Published models place them at roughly 8–21 atm. Pressures of a few thousand atmospheres (kilobars) are reached only far below the cloud decks, deep in the molecular envelope. Table 1 records this and the other magnitude checks.

3.4 The molecular H_2–He envelope (≈20 bar to ≈1 Mbar; up to ≈10^6 atm)

Below the clouds lies a deep, convective envelope of molecular hydrogen and helium. Pressure and temperature rise together along a roughly adiabatic profile, through the kilobar (10^3 atm) and 10–100 GPa (10^5–10^6 atm) ranges. Shock experiments show that fluid hydrogen becomes increasingly conducting with depth, well before full metallisation (Nellis et al., 1996). Modelling cited by Mankovich and Fuller (2021) expects conductivities of order 10^4 S/m deeper than about 10^6 bar (Liu et al., 2014). Saturn's zonal winds extend to a depth of about 9,000 km (Iess et al., 2019; Militzer and Hubbard, 2023).

3.5 The metallic-hydrogen transition (≈0.8–2 Mbar; ≈80–200 GPa; ≈0.8–2 × 10^6 atm)

At about 1–2 Mbar, hydrogen in giant planets changes continuously from a molecular, insulating fluid to an atomic, metallic fluid. Laboratory experiments locate this insulator-to-metal transition in dense fluid deuterium at roughly 150–250 GPa below 2000 K (Celliers et al., 2018); a Z-machine study found it near 300 GPa at the temperatures it covered (Knudson et al., 2015). In Saturn, models predict that helium becomes immiscible in metallic hydrogen ("helium rain") starting at about 80–100 GPa (Militzer and Hubbard, 2023), as theory long predicted (Stevenson and Salpeter, 1977; Morales et al., 2009; Schöttler and Redmer, 2018) and experiments support (Brygoo et al., 2021). Temperatures near 1–2 Mbar are about 6,500 K in a representative model profile (Fortney et al., 2023). The informal claim that "millions of atmospheres" are reached near the metallic transition is **confirmed**: 1–2 Mbar ≈ 1–2 × 10^6 atm.

3.6 The fuzzy (dilute) core (≈1–10 Mbar and deeper)

Cassini gravity measurements imply a core of roughly 15–18 $M_\oplus$ (Iess et al., 2019); other models allow about 12–20 $M_\oplus$ (Fortney et al., 2023). Ring seismology, which uses waves in the rings excited by oscillations in Saturn, shows that the core is not compact. It is a diffuse, stably stratified region extending to about 0.59 of Saturn's radius, holding about 55 $M_\oplus$ of material including about 17 $M_\oplus$ of ice and rock, with a composition gradient across about 1–10 Mbar (Mankovich and Fuller, 2021). Jupiter shows a similar dilute-core picture from Juno (Wahl et al., 2017; Bolton et al., 2017; Stevenson, 2020); that comparison is context only. A schematic adiabatic profile reaches about 10^4 K near 10 Mbar (Fortney et al., 2023), and if

the core is stably stratified the central temperature could be a few times higher (Mankovich and Fuller, 2021). **Temperature verification:** "10,000+ K" is therefore supported only as an order-of-magnitude value for the deep interior (≈10 Mbar and below), with a model range of about 10^4 K to a few × 10^4 K. It is not a value for the metallic transition (≈6,500 K) or for any depth a probe could reach.

Layer / claim	Informal estimate	Published range (atm ≈ bar)	Status
Deep water clouds	"thousands of atm"	≈8–21 bar ≈ 8–21 atm (Del Genio et al., 2009; Mousis et al., 2014)	**Corrected**
Metallic-H transition	"millions of atm"	≈0.8–2 Mbar ≈ 0.8–2 × 10^6 atm (Militzer and Hubbard, 2023; Celliers et al., 2018)	Confirmed
Deep-interior temperature	"10,000+ K"	≈6,500 K at 1–2 Mbar; ≈10^4 K near 10 Mbar; possibly a few times higher at centre (Fortney et al., 2023; Mankovich and Fuller, 2021)	Partly confirmed; range
Kilobar (10^3 atm) levels	(implicit)	Deep in the molecular envelope, far below all clouds (INFERENCE from the adiabatic profile)	Clarified

Table 1: Magnitude checks of the informal estimates that motivated this paper.

4 Core Hypothesis: Nested Sacrificial Shells

HYPOTHESIS Each node is a set of concentric shells. Each shell is matched to one pressure–temperature–chemistry band and is expected to fail, or to be deliberately shed, once its band is exceeded, exposing an inner shell built for the next band. The aim is not survival to great depth but a predictable sequence of functional states, each long enough to take and relay measurements in its band. The idea borrows the logic of staging from launch vehicles and of sacrificial heat shields such as Galileo's ablative forebody (Milos, 1997). Whether ceramic shells can be made to fail in a controlled, staged way at this scale is UNTESTED.

The shell bands follow the layers in Section 3:

- **S1 (cruise to ≈2 bar).** A lightweight outer skin for handling, descent stability, and the cold NH_3 cloud environment (≈130–150 K).
- **S2 (≈2.5–5 bar).** Resistance to NH_4SH and sulphur chemistry.
- **S3 (≈8–21 bar).** Pressure and aqueous-ammonia exposure in the water-cloud band, at temperatures rising toward and above 0 °C.
- **S4 (design target 10^2–10^3 bar).** A dense inner pressure shell. This is far beyond Galileo's ≈22 bar, and whether a small sphere can operate there long enough to relay is the central UNTESTED question. Even 10^3 bar is only 0.1 GPa, three orders of magnitude below the metallic transition.

No shell in this architecture is expected to reach or operate in the metallic-hydrogen region (≈100 GPa). The cover art and Figure 8 show that destination conceptually; physically, nodes are lost long before. Their data describe the path toward that boundary, not the boundary itself. Appendix A.4 quantifies the shell-stress limits.

5 Golf-Ball Probe Design

In this paper "golf-ball" refers only to **size and form**: a sphere 43 mm across (a regulation golf ball is about 42.7 mm) with an assumed mass of order 0.1 kg. It does not imply dimpling or any aerodynamic property of golf balls. Figure 2 shows the shells and the core.

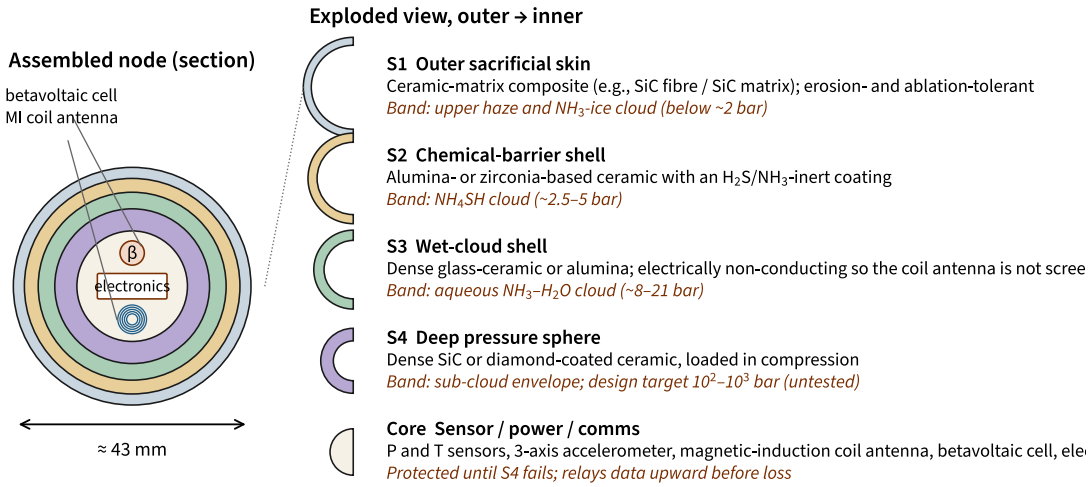


Figure 2: Exploded view of a concept node (≈43 mm). Left: assembled section with a radioisotope or primary-cell power element, electronics, and a magnetic-induction/radio coil. Right: candidate shell materials by band. Shells S3 and S4 are specified as non-conducting ceramics so that they do not screen the antenna. Materials are illustrative and there are no test data (UNTESTED).

The core carries a minimal sensor set chosen by mass and power (pressure, temperature, and possibly a simple optical or conductivity sensor), a clock, a few kilobytes of memory, and a radio/induction front end. A sphere has the smallest surface area for its volume, which suits a pressure vessel, and has no preferred orientation, which simplifies the antenna if the coil is close to isotropic. These are engineering inferences (INFERENCE), not test results.

Shell materials are candidates only: S1 a SiC/SiC ceramic-matrix composite; S2 alumina or zirconia with an inert coating; S3 a glass-ceramic or alumina; S4 dense SiC or a diamond-coated ceramic. Conducting metal shells are avoided around the antenna, because a closed metal sphere would screen the low-frequency fields the deeper links rely on (Section 8), as follows from skin-depth physics (Jackson, 1999).

Atmospheric entry is not survivable for an unprotected 43 mm sphere without a substantial ablator (Appendix A.6). Galileo's probe needed a massive heat shield that ablated heavily (Milos, 1997). The baseline therefore assumes that all nodes ride inside a single shared aeroshell and are released only after the aeroshell is jettisoned and a dispenser is descending under a parachute (Figure 8), as Galileo's probe did. The total node mass for 10,000 nodes at 0.1 kg is about 1,000 kg, roughly three times the 339 kg Galileo probe (Mousis et al., 2014). ORDER-OF-MAGNITUDE DESIGN ESTIMATE, NOT A DERIVED MISSION REQUIREMENT

6 Mesh Network Bus Architecture

HYPOTHESIS The dispenser releases nodes one at a time at an interval Δt. Each node falls at its terminal velocity, takes measurements, and passes its own data, together with the data from the node below it, to

the node above. The node nearest the dispenser passes the aggregated stream to the dispenser, which relays it on UHF to the orbiter (Figure 3). As the deepest node fails, the next becomes the head of the chain; as new nodes are released at the top, the chain is renewed. An initial tranche of 10,000 nodes is proposed as a design choice for discussion, not derived from a requirement.

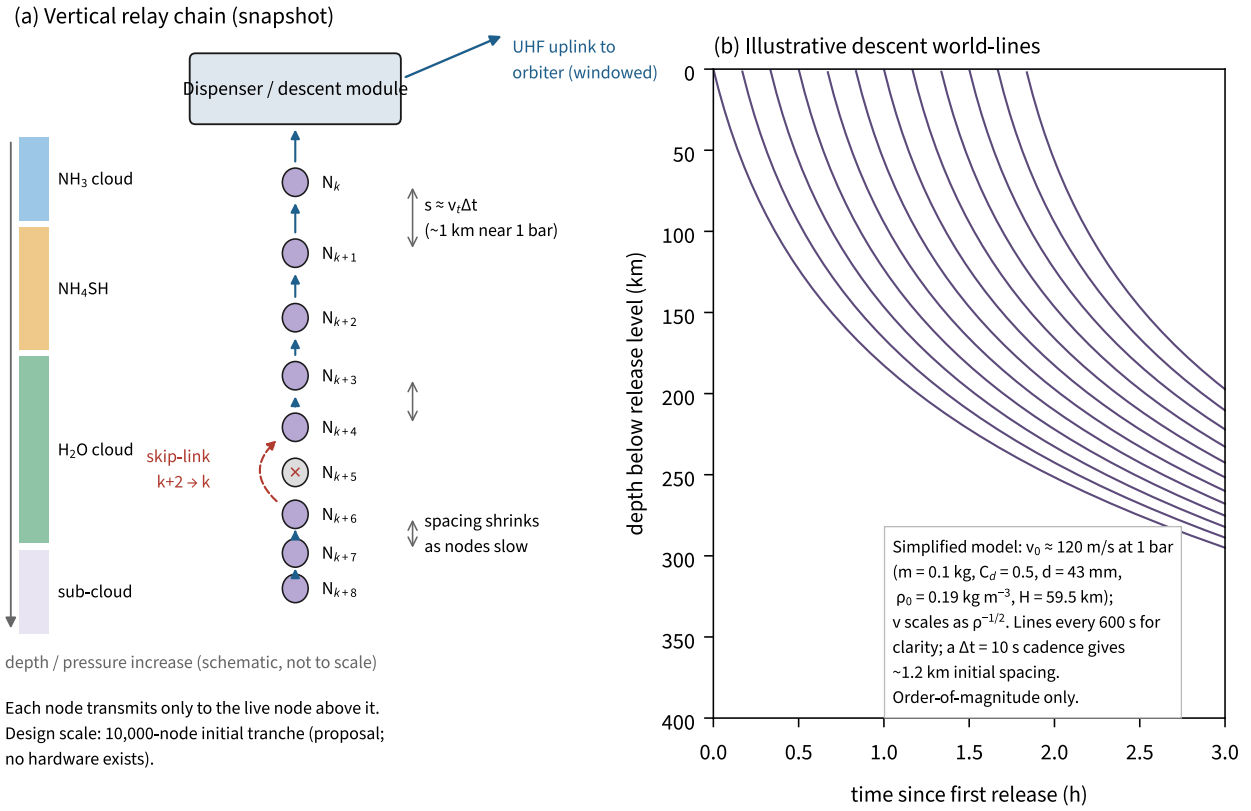


Figure 3: Mesh bus concept. (a) Snapshot of the chain: each node N_k relays upward to N_{k-1} if a node fails (×), the next uses a skip-link to the one beyond it. Spacing shrinks with depth as nodes slow. (b) Node depth versus time from the simplified descent model of Equation 2 with release interval Δt = 10 s. Proposal only; no hardware exists.

For a sphere of mass m, drag coefficient C_d, and cross-section A in gas of density ρ, the terminal velocity is

$$v_t = \sqrt{\frac{2mg}{\rho C_d A}}. \tag{1}$$

With m = 0.1 kg, $g \approx 10$ m/s², $C_d \approx 0.5$ and $A = 1.45 \times 10^{-3}$ m², Equation 1 gives $v_t \approx 120$ m/s at the 1-bar density of 0.19 kg/m³, ≈52 m/s at 1 kg/m³, ≈23 m/s at 5 kg/m³, and ≈12 m/s at 20 kg/m³. These are ESTIMATE values: they assume a constant drag coefficient and ignore winds and turbulence, which Galileo found to be strong (Young, 2003). In an isothermal atmosphere with scale height H, density grows exponentially with depth, so v_t falls as $e^{-z/2H}$. Integrating gives the depth below the release level,

$$z(t) \approx 2H \ln\left(1 + \frac{v_0 t}{2H}\right), \tag{2}$$

with $H \approx 59.5$ km (Williams, n.d.) and v_0 the terminal velocity at release. The isothermal assumption is crude because temperature rises with depth; Equation 2 is used only for Figure 3, panel (b), and Appendix A.2.

The number of nodes alive at once is roughly $N_{live} \approx \tau/\Delta t$, where τ is a node's functional lifetime. With τ = 1 h and Δt = 10 s, about 360 nodes would be alive at once. Releasing 10,000 nodes at Δt = 10 s takes about

10^5 s (≈28 h), so the dispenser must survive and stay in contact for that long, or be replaced by staged dispensers; both are UNTESTED. Routing can be very simple: each node only needs to reach the next node up, with a skip-link to the node two above as a fallback. This store-and-forward idea is borrowed from terrestrial wireless sensor networks; applying it to a falling chain is HYPOTHESIS. Appendix A.3 quantifies its reliability.

7 Power

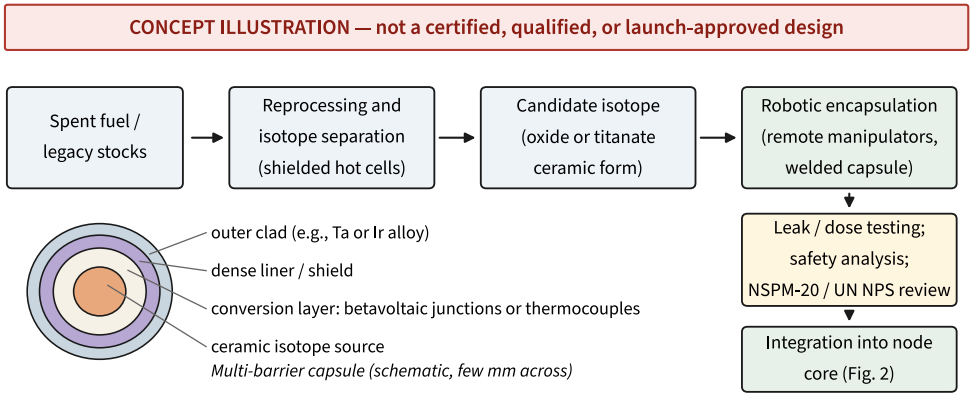
Each node needs microwatts to milliwatts for a lifetime of minutes to hours. Two power classes are considered.

Primary chemical cells. For lifetimes of hours, a small primary battery is probably the simplest and safest choice. This is an engineering judgement (INFERENCE); a rigorous comparison is left open. A radioisotope source is attractive only if nodes or the dispenser must stay powered through a long cruise or dispensing campaign.

Radioisotope sources. Several points must be stated carefully (Figure 4, Table 2).

1. **Spacecraft RTGs use Pu-238 made on purpose.** Pu-238 is produced by irradiating neptunium-237 targets in a reactor and chemically separating the product in shielded hot cells; the separated mixture is about 10–15% Pu-238, which is then made into ceramic oxide pellets clad in iridium (Idaho National Laboratory, n.d.; NASA, n.d.-d). It is an alpha emitter and is not weapons-grade material (NASA, n.d.-d).
2. **Spent-fuel plutonium is not a drop-in RTG fuel.** Plutonium from typical light-water-reactor spent fuel is only about 2% Pu-238; the rest is mainly Pu-239, Pu-240 and Pu-241 (World Nuclear Association, n.d.). Isotope separation of plutonium is not a practical route to Pu-238. The honest “waste-derived” path is americium-241, which builds up in aged civil plutonium as Pu-241 decays and is being developed for European radioisotope power (World Nuclear Association, n.d.).
3. **Cs-137 is a poor choice.** Its decay emits a 662 keV gamma ray in about 85% of decays (LNHB, n.d.; U.S. EPA, n.d.-a). Shielding that radiation would dominate the mass of a small node.
4. **Sr-90 is a candidate for betavoltaic or small thermal sources.** It is a beta emitter with a half-life of about 29 years, present in reactor wastes (U.S. EPA, n.d.-b; LNHB, 2005a). Its energetic Y-90 daughter produces bremsstrahlung that needs some shielding (INFERENCE). Betavoltaic cells give long-lived but low power at low efficiency (Olsen et al., 2012; Zhou et al., 2021).
5. **Regulation.** Any U.S. launch with radioisotope sources falls under NSPM-20′s tiered authorization, with tiers set by the total activity in multiples of the IAEA A_2 value and by accident-dose probabilities (The White House, 2019). International use is guided by the 1992 UN Principles (United Nations, 1992). A swarm of 10,000 sources is a novel case for safety analysis and public acceptance.

Nuclear waste must not be oversold as “fuel” for this concept. Separation, encapsulation, qualification and launch approval are each major programmes in their own right (National Research Council, 2009). Figure 4 shows the chain of steps.



Isotope	Half-life	Decay	Assessment for this concept
Pu-238	88 y	α	RTG standard; made by irradiating Np-237, not taken from spent-fuel Pu
Am-241	long-lived	α (+γ)	recoverable from aged civil Pu; route being developed for European RPS
Sr-90	29 y	β	fission product in reactor waste; betavoltaic candidate (bone-seeking hazard)
Cs-137	≈30 y	β + strong γ	poor choice: high-energy γ demands heavy shielding
Spent-fuel Pu	mixed	mostly α	≈2% Pu-238 in typical LWR spent-fuel Pu; not a drop-in RTG fuel

Sources: World Nuclear Association; NASA RPS Program; ORNL; U.S. EPA (see Sec. 7 and References).

Figure 4: Concept of a waste-derived power path and multi-barrier capsule, with an isotope comparison. Concept illustration only, not a qualified or approved design. Sources: World Nuclear Association (n.d.), NASA (n.d.-d), Idaho National Laboratory (n.d.), U.S. EPA (n.d.-b), U.S. EPA (n.d.-a); regulatory steps per The White House (2019) and United Nations (1992).

Sizing estimate. From LNHB decay data (half-life 28.80 a; mean beta energies 196 keV for Sr-90 and 926.7 keV for Y-90) (LNHB, 2005a; LNHB, 2005b), Sr-90 in equilibrium with Y-90 releases about 0.92 W of heat per gram (ESTIMATE ; Appendix A.5). A 10 mg source gives about 9 mW of heat; at a betavoltaic total efficiency of 0.2–2% (an assumed range informed by Zhou et al. (2021)) that is about 0.02–0.2 mW electrical. For 10,000 nodes the total would be about 100 g of Sr-90, or about 5×10^{14} Bq, whose NSPM-20 tier would have to be determined formally. ORDER-OF-MAGNITUDE DESIGN ESTIMATE, NOT A DERIVED MISSION REQUIREMENT Thermoelectric conversion also worsens as the atmosphere heats, because the available temperature difference shrinks.

Isotope	Half-life	Decay	Assessment
Pu-238	≈88 y	α	Standard RPS fuel; made from Np-237 (Idaho National Laboratory, n.d.; World Nuclear Association, n.d.)
Am-241	long	α (+ weak γ)	Recoverable from aged civil Pu; European RPS route (World Nuclear Association, n.d.)
Sr-90	28.80 a	β (Y-90 β)	Betavoltaic candidate; reactor waste (LNHB, 2005a; U.S. EPA, n.d.-b)
Cs-137	30.02 a	β, strong γ	Poor choice: 662 keV γ shielding mass (LNHB, n.d.)
Spent-fuel Pu	mixed	mostly α	≈2% Pu-238; not a drop-in RTG fuel (World Nuclear Association, n.d.)

Table 2: Candidate isotopes for node or dispenser power.

8 Signal Strategy

Three link families are compared (Figure 5, Table 3): ELF/VLF (3 Hz–30 kHz) and the related magnetic-induction (MI) near-field links; medium frequency through UHF (the "AM/FM" family, about 0.3 MHz to 3 GHz); and optical (laser) links.

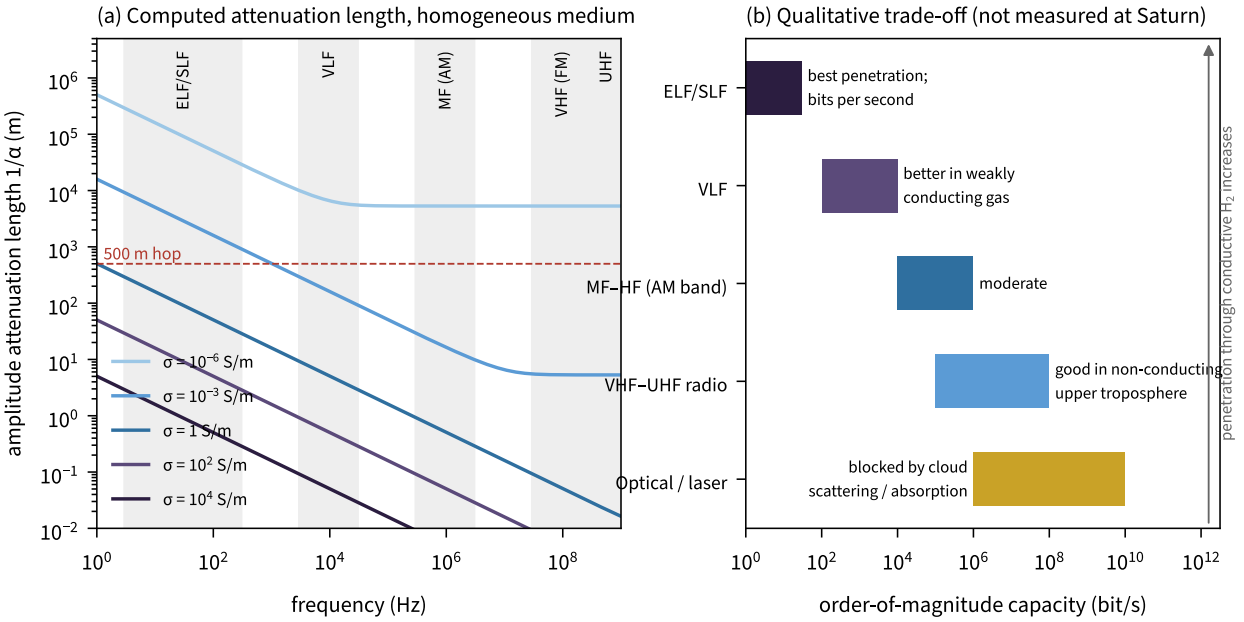


Figure 5: Signal comparison. (a) Attenuation length 1/α versus frequency, calculated from the standard plane-wave expression for a medium of conductivity σ (Jackson, 1999), for σ from 10^{-6} to 10^{4} S/m. The horizontal line marks a 500 m hop. (b) Qualitative data-rate ranges per band; illustrative (INFERENCE), not link budgets.

Physics. In a conducting medium the field amplitude falls as $e^{-z/\delta}$. In the good-conductor limit the skin depth is

$$\delta = \frac{1}{\sqrt{\pi f \mu_0 \sigma}} \approx \frac{503}{\sqrt{\sigma f}} \ \text{m}, \tag{3}$$

with σ in S/m and f in Hz (Jackson, 1999). At σ = 10^{4} S/m, the value expected deep in the envelope (Mankovich and Fuller, 2021; Liu et al., 2014), even 100 Hz penetrates only about 0.5 m. At σ = 1 S/m, 10 Hz gives about 160 m and 3 kHz about 9 m. Low frequencies always penetrate a conductor best, which is why ELF/VLF are the established choice for reaching through seawater and the ground (Barr et al., 2000).

Where each band fits. In the upper, cold, non-conducting troposphere the main loss at radio frequencies is absorption by ammonia and water rather than conductivity. Galileo relayed data at UHF/L-band to about 22 bar with measurable ammonia attenuation (Folkner et al., 1998), and Mousis et al. (2014) note that radio opacity increases beyond about 10 bar. INFERENCE The recommended plan is UHF/L-band for the upper chain and dispenser uplink, and ELF/VLF or MI for the deepest node-to-node hops, where the gas becomes partly conducting and microwave absorption is severe. Optical links are ruled out in the cloud decks by scattering and kept only above the clouds, if at all.

Honest trade-off. A 43 mm coil is tiny compared with an ELF wavelength (3,000–100,000 km) or a VLF wavelength (10–100 km). It cannot radiate efficiently and works as a near-field MI link, whose signal falls off steeply with distance (Sun and Akyildiz, 2010). Appendix A.1 quantifies this: with stated assumptions, a golf-ball coil pair at 1 mW closes only about 7 m at 1 kHz, even in a perfectly insulating gas. Hops of hundreds of metres would need tens of kilowatts or more, or much larger relay-class coils (UNTESTED).

Bandwidth is the other penalty. The Shannon limit, $C = B\log_2(1 + \mathrm{SNR})$, caps a link with only tens of hertz of usable bandwidth at roughly 10–100 bit/s even at good SNR, enough for a few pressure and temperature samples per minute, not imaging (INFERENCE).

Band	Penetration	Indicative data rate	Role in this architecture
ELF/SLF (3 Hz–3 kHz)	Best in conductors	≈1–30 bit/s	Deepest hops only; open feasibility
VLF (3–30 kHz)	Good	$\approx 10^2$–10^4 bit/s	Deep hops; MI near-field
MF–HF (0.3–30 MHz)	Moderate	$\approx 10^4$–10^6 bit/s	Backup mid-chain
VHF–UHF/L (30 MHz–3 GHz)	Good in dry, non-conducting gas; NH_3 absorption	$\approx 10^5$–10^8 bit/s	Upper chain; dispenser-to-orbiter (Galileo precedent)
Optical	Blocked by clouds	$\approx 10^6$–10^{10} bit/s	Above clouds only, if at all

Table 3: Link families compared. Data rates are indicative orders of magnitude (INFERENCE), not link budgets.

9 Material Science Frontier

The deepest target in this paper, 10^2–10^3 bar, is modest by laboratory standards. Static diamond-anvil cells (DACs) squeeze a sample between two diamond tips, called culets, tens to hundreds of micrometres across, inside a metal gasket; pressure is read from the fluorescence of a ruby chip or the X-ray lattice spacing of a gold marker. With two-stage nanodiamond anvils, DACs have reached about 640 GPa (Dubrovinsky et al., 2012). Dynamic compression by lasers or pulsed power now covers the whole pressure range of Saturn's interior (Duffy and Smith, 2019; Fortney et al., 2023). Figure 7 sketches both techniques.

High pressure also changes chemistry in ways that can be summarised as a "high-pressure periodic table" (Figure 6). Sodium becomes an optically transparent insulator near 200 GPa (Ma et al., 2009). Lithium turns from a metal into a semiconductor near 80 GPa (Matsuoka and Shimizu, 2009). Oxygen becomes metallic near 95–96 GPa (Desgreniers et al., 1990; Akahama et al., 1995) and superconducts at about 0.6 K near 100 GPa (Shimizu et al., 1998). Helium, normally inert, forms the stable compound Na_2He above 113 GPa (Dong et al., 2017). Hydrogen becomes metallic near 150–250 GPa in dense fluid deuterium (Celliers et al., 2018; Knudson et al., 2015) and separates from helium under giant-planet conditions (Brygoo et al., 2021). A wider review is given by Mao et al. (2018).

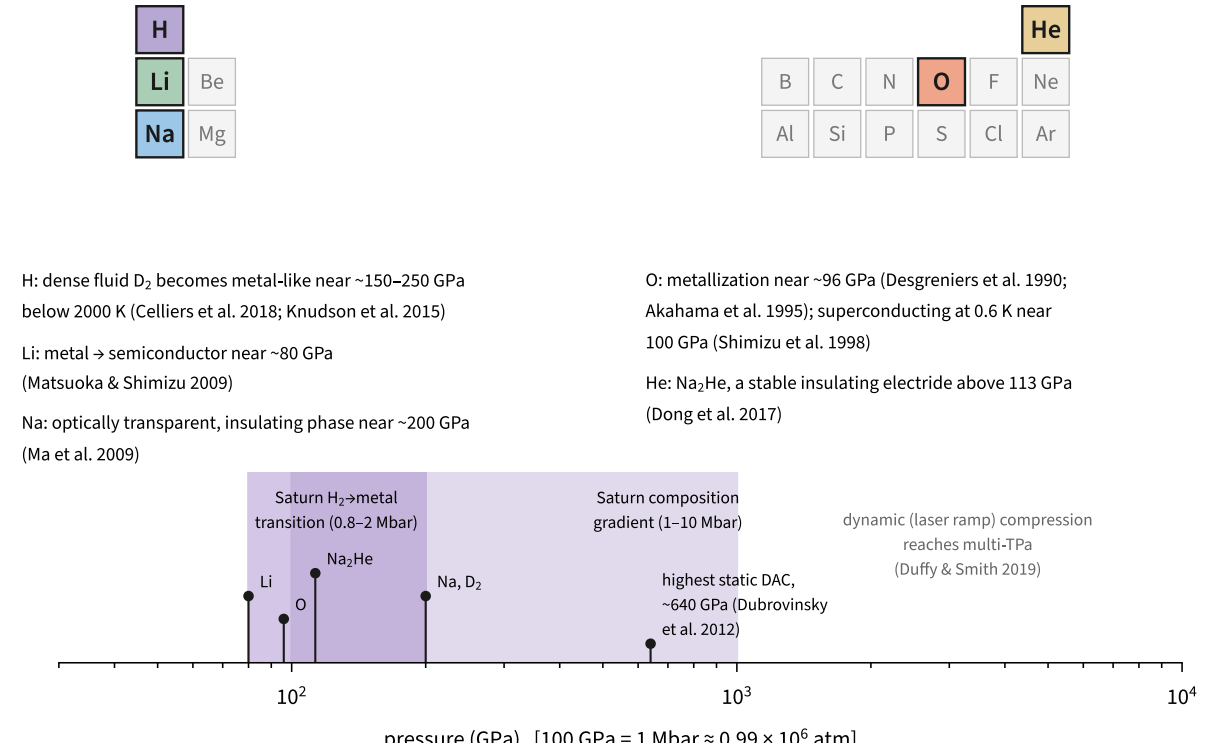


Figure 6: A “high-pressure periodic table” concept: selected light elements whose behaviour changes under compression, set against the pressures of Saturn’s transition region and composition gradient. Values are from the studies cited in the figure and text; the Saturn bands are model-dependent (Militzer and Hubbard, 2023; Mankovich and Fuller, 2021).

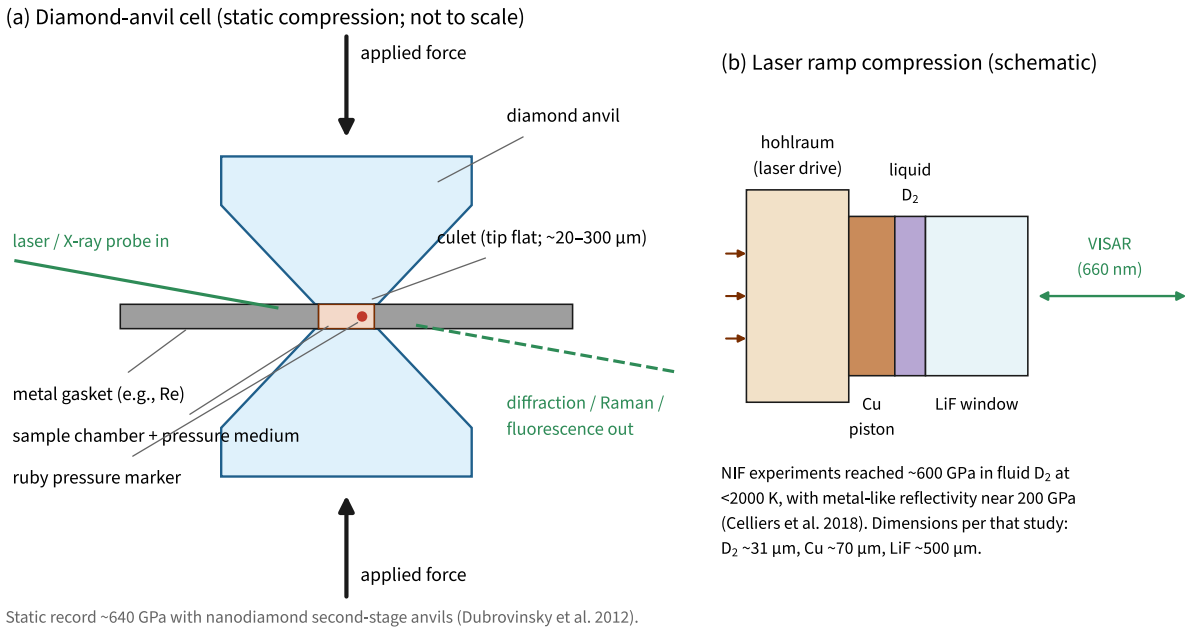


Figure 7: Laboratory analogues. (a) Schematic diamond-anvil cell, not to scale, after Dubrovinsky et al. (2012). (b) Laser ramp-compression target after Celliers et al. (2018): a laser-driven hohlraum pushes a copper piston into a thin layer of liquid D_2 backed by a LiF window, monitored by a VISAR interferometer at 660 nm.

Relevance to the probe. First, these results set the scientific goal: the deepest data a node chain could return would constrain the upper boundary conditions for these deep regimes, not the regimes themselves. Second, they caution against assuming that any material keeps its familiar properties once conditions change by large factors. Shell materials for S3–S4 would need qualification at 10^2–10^3 bar and ≈300–1,000 K in hydrogen, ammonia and water. No such data exist for this concept (UNTESTED), and the temperature range itself is an INFERENCE extrapolated from the adiabatic trend between the cloud decks and the Mbar values above.

10 Enhancements

Swarm economics. HYPOTHESIS Ten thousand identical small units may cost less per measurement than a single bespoke probe, because of manufacturing learning curves, and they tolerate individual failures. No cost model exists for this concept; the claim should be tested with a parametric cost study.

Band specialisation. Nodes need not be identical. Upper-band nodes could carry UHF radios and lighter shells, while a subset of heavier relay-class nodes with larger coils carries the deep VLF/MI hops identified as the weak point in Section 8 (HYPOTHESIS).

Uplink windows. Saturn rotates in about 10 h 33 min (Mankovich and Fuller, 2021), and zonal winds of up to about 400 m/s carry the dispenser in longitude (Williams, n.d.). The orbiter will therefore be in view of the dispenser only during windows: the chain should buffer and burst its data to the dispenser, which stores data and sends it upward when the orbiter is in view (INFERENCE). Galileo's probe relayed to its orbiter overhead in a similar way (Young, 1998).

Node spacing: hundreds of metres to about 1 km.

ORDER-OF-MAGNITUDE DESIGN ESTIMATE, NOT A DERIVED MISSION REQUIREMENT

The spacing between consecutive nodes is $s \approx v_t \Delta t$. Near 1 bar, $v_t \approx 120$ m/s, so $\Delta t = 5$–20 s gives $s \approx 0.6$–2.4 km; deeper, at about 5 kg/m^3, the same interval gives about 0.1–0.5 km. Three considerations bound the choice:

1. The spacing must not exceed the reliable link range, set by attenuation (Figure 5) and the link budget (Appendix A.1).
2. Spacing that is too small wastes nodes and causes interference between neighbours.
3. The number of nodes alive at once, $N_{live} \approx \tau/\Delta t$, must keep the chain connected despite failures (Appendix A.3).

Together these suggest hundreds of metres to about 1 km for UHF links in the upper troposphere; this is the origin of the figure and its sole rationale. Appendix A.1 shows that deep MI hops of that length are not achievable with golf-ball coils, so in the deep regime either spacing must shrink to metres–tens of metres or relay-class nodes are required.

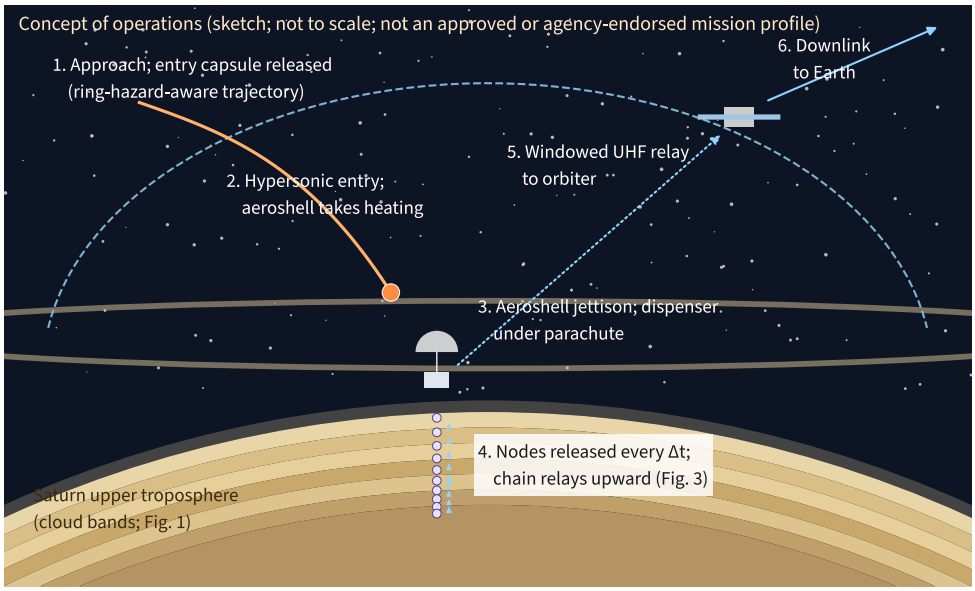


Figure 8: Concept of operations from orbiter to swarm: (1) approach and capsule release on a ring-hazard-aware trajectory (Mousis et al., 2014); (2) entry inside a shared aeroshell; (3) aeroshell jettison and parachute-borne dispenser; (4) nodes released every Δt, forming the relay chain (Figure 3); (5) UHF relay to the orbiter during visibility windows; (6) downlink to Earth. Sketch only, not to scale; not an approved or agency flight profile.

11 Iterative Descent: The Closed Feedback Loop

UNTESTED This section proposes a **research programme**, not a demonstrated capability. Its logic is that each generation of probes should go only as deep as current Earth materials can withstand, and that what it learns should determine how the next generation is built.

Stay within proven materials. No generation of nodes attempts to breach layers beyond what qualified Earth materials can survive. In the stress model of Appendix A.4, room-temperature metals and engineering ceramics in a golf-ball shell reach their limits at about 10^3–10^4 atm. A first generation would therefore target the cloud decks and the upper molecular envelope (≈1–10^3 bar), where Galileo-class heritage and conventional ceramics apply.

Each band returns a materials blueprint. Each node collects elemental and structural data from its assigned band (pressure, temperature, composition where instruments allow, and telemetry on how and when its own shell failed) and transmits them upward through the mesh. The failure telemetry is as valuable as the atmospheric data: it tells designers which shell failed, at what pressure and temperature, and how quickly.

Earth laboratories synthesise the next shell. The returned conditions become targets for laboratory work: diamond-anvil-cell and laser-compression experiments (Dubrovinsky et al., 2012; Duffy and Smith, 2019; Celliers et al., 2018), guided by computational models and machine-learning-assisted ("AI-assisted") searches over candidate compositions and processing routes. The aim is to find or make materials that survive the next band's conditions. HYPOTHESIS

The next generation goes one band deeper. Once a material has been synthesised **and** manufactured at shell scale and qualified, the next generation of nodes is built from it and targets one band deeper. Saturn reveals what conditions exist at each depth; Earth makes materials for them; new probes descend further; and the exploration boundary moves inward one shell at a time (Figure 9).

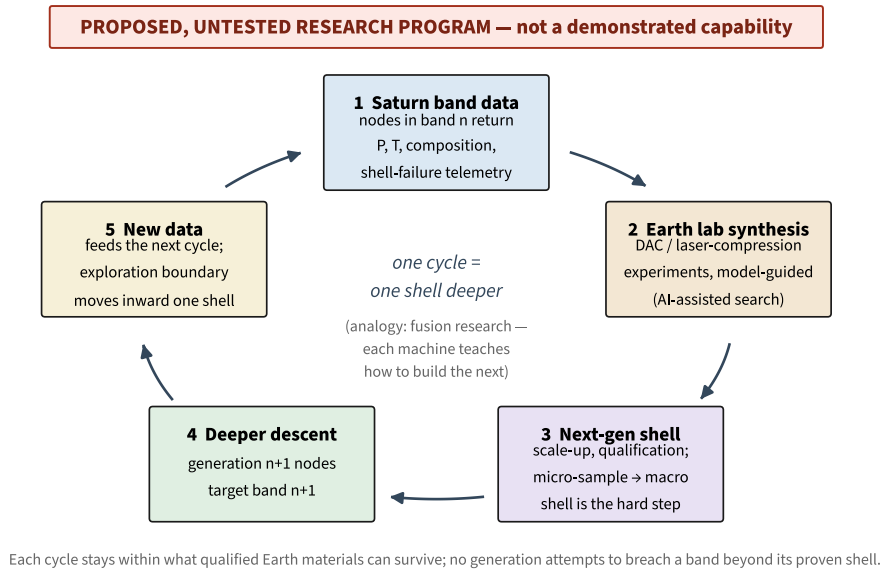


Figure 9: The closed feedback loop of iterative descent: Saturn band data → Earth-laboratory synthesis → next-generation shell material → deeper descent → new data. Proposed, untested research programme; step 3 (from a laboratory micro-sample to a macroscopic, qualified shell) is the hardest and least certain step.

An honest caveat. Synthesising a high-pressure phase in a DAC or a laser shot is not the same as manufacturing a structurally useful probe shell. DAC samples are micrometres across (Dubrovinsky et al., 2012); laser ramp-compression targets are tens of micrometres thick and exist at peak pressure for nanoseconds (Celliers et al., 2018). Many high-pressure phases are not recoverable at ambient conditions. Even recoverable materials must then be made in bulk, shaped into a 43 mm shell, and qualified against hot, hydrogen-rich, chemically aggressive gas. Each loop may take years. The programme succeeds only if that scale-up step succeeds for at least some materials, and that is unknown.

Analogy with fusion research. Fusion research has not been solved in one step; each experimental machine has informed the design of the next. The iterative descent loop has the same character: build a machine that teaches you how to build the next machine. The analogy concerns method, not timescale or likelihood of success.

12 Limitations and Open Problems

1. **Link closure deep in the chain** is the biggest open problem. Appendix A.1 shows that golf-ball MI coils close only metre-to-tens-of-metres hops at milliwatt power (ESTIMATE).
2. **Shell staging** has no test data; controlled, staged failure of ceramic shells at 43 mm scale has not been demonstrated (UNTESTED).

3. **Entry and dispensing** of 10,000 nodes from one aeroshell over about 28 hours exceeds any flown capability; staged dispensers may be needed.
4. **Winds and turbulence** will scatter nodes horizontally as well as vertically, straining the simple vertical-chain picture (Young, 2003).
5. **Mass:** about 1 t of nodes alone, plus aeroshell, dispenser and orbiter, is large, and the rings are a hazard on approach (Mousis et al., 2014).
6. **Radioisotope options** face regulatory, safety and public-acceptance hurdles (The White House, 2019; United Nations, 1992); chemical power may be preferable.
7. **Science return per node** is small (a few bit/s at depth), so instruments must be minimal, and an ELF hop cannot keep pace with a 10 s release cadence (Appendix A.2).
8. **Interior models** differ, so target depths and conditions carry model ranges (Militzer et al., 2019; Fortney et al., 2023).
9. **The iterative loop** depends on scaling laboratory high-pressure materials to macroscopic shells, which is unproven (Section 11).

13 Conclusion

This paper set out a hypothesis-driven architecture for exploring Saturn's atmosphere with a sequential swarm of sacrificial, golf-ball-sized nodes linked as a descending relay mesh, and an iterative programme in which each generation's data shape the next generation's materials. Placed against the published science, the concept has sound features: it targets a world that has never had an entry probe, uses an entry sequence and an upper-atmosphere UHF relay with Galileo precedent, and aims at depths (10^2–10^3 bar) that are modest in pressure terms but beyond any probe to date. It also has clear weak points, quantified in Appendix A. Golf-ball MI links are very short-ranged. Shell staging is untested. Dispensing is unprecedented. A series relay chain is brittle without redundancy. Bare-node entry would need a large ablator fraction. Radioisotope power raises regulatory problems that rule out casual reliance on "nuclear waste". The most useful next steps are a link-budget and antenna study for relay-class deep nodes, coupon tests of candidate ceramics in hot, high-pressure ammonia–water–hydrogen environments, and a parametric comparison of swarm and single-probe architectures. I offer the concept so that it can be tested and corrected.

14 Path to Funding and Next Steps

This white paper is the opening argument: **theory first, hardware second, data third.** The real trial begins when the first node drops. The routes below are realistic starting points; none has been applied to yet, and circulating this document does not constitute a proposal to any agency.

NASA Innovative Advanced Concepts (NIAC). NIAC funds early-stage, visionary concepts. NASA currently lists Phase I as **$225,000 for a nine-month study** (12–18 awards per year planned), Phase II as $750,000 for two years, and Phase III as $2 million for two years; these are tentative figures stated by NASA (NASA, n.d.-e). (An earlier informal figure of $125,000 for Phase I is outdated; see Section 15.) Solicitations are released through NSPIRES. The 2027 Phase I solicitation was released on 28 September 2026 (NASA, n.d.-e), with a two-step process (a short Step A proposal, then an invited Step B) and submission by an authorized organizational representative (NASA STMD, 2026). Eligibility matters here: U.S. organizations may apply, while non-U.S. organizations may partner in or lead studies only on a no-exchange-of-funds basis (NASA STMD, 2026). An independent researcher in The Bahamas would therefore most plausibly participate through a U.S. partner organization. The role of this paper is as the technical foundation for a future NIAC Step A proposal, not as an application.

European Space Agency: OSIP and the Advanced Concepts Team. ESA's Open Space Innovation Platform (OSIP) is the entry point for novel ideas into ESA's Discovery activities. Ideas are submitted to themed Campaigns or open Channels, including an open Discovery channel; the best are invited to full proposals, and funding typically takes the form of co-funded PhD or post-doctoral research, early technology development, or system studies (European Space Agency, n.d.-a; European Space Agency, n.d.-b). ESA's Discovery element also includes the Advanced Concepts Team, a future-oriented research team (European Space Agency, n.d.-c). OSIP accepts ideas from individuals as well as organizations (European Space Agency, n.d.-b); whether a particular call admits a non-European lead must be checked call by call.

DARPA and defense-sector materials research. Materials that survive extreme pressure, temperature and chemistry have dual-use relevance. DARPA's Defense Sciences Office lists "Materials, Manufacturing, and Energy Systems" among its thrust areas (DARPA, n.d.). The appropriate framing is modest: the materials-qualification and high-pressure-synthesis parts of Section 11 could align with such programmes, subject to their own solicitations, eligibility rules and export-control constraints. They are not a funding source for a Saturn mission as such.

Public support and crowdfunding. The author's existing media platforms, Bahama Drama and lol242.com, can be used to tell the story, pre-sell accessible products (for example, an illustrated edition of this paper), and build a public base before hardware money is needed. Crowdfunding cannot pay for flight hardware, but it can fund small, verifiable steps: an open link-budget simulation, a coil prototype test, or a peer review of this paper by specialists.

Proposed sequence (ESTIMATE). (1) Expert review and correction of this paper. (2) A NIAC- or OSIP-scale study focused on the deep-link problem and node-level entry and stress analysis. (3) Laboratory coupon tests of shell materials. (4) Only then, any discussion of flight hardware, in partnership with an institution able to carry a mission.

15 Notes on Uncertainties and Factual Corrections

This section lists every correction, uncertainty, extrapolation, and partly verified source used in the paper.

15.1 Corrections to earlier informal estimates

1. **Water-cloud pressure.** "Thousands of atm" is corrected to ≈8–21 bar (≈8–21 atm), depending on the assumed O/H (Del Genio et al., 2009; Mousis et al., 2014). Kilobar pressures are reached only deep in the molecular envelope.
2. **Metallic-transition pressure.** "Millions of atm" is confirmed: ≈0.8–2 Mbar ≈ $0.8–2 \times 10^6$ atm (Militzer and Hubbard, 2023).
3. **Deep temperature.** "10,000+ K" holds only as about 10^4 K near 10 Mbar in adiabatic models, possibly a few times higher if the core is stably stratified (Fortney et al., 2023; Mankovich and Fuller, 2021); it is about 6,500 K at the metallic transition. Fortney et al.'s values are read from a schematic figure in a preprint and are approximate.
4. **NIAC Phase I amount.** The informal figure of $125,000 is outdated. NASA's NIAC page lists Phase I at $225,000 for a nine-month study (tentative) (NASA, n.d.-e).

15.2 Uncertain or model-dependent values

1. **Interior quantities** (core mass, dilute-core extent, transition depth, temperatures) are model-dependent; core-mass estimates range from about 12 to 20 $M_\oplus$ (Iess et al., 2019; Fortney et al., 2023).

2. **The 1-bar temperature** is given as 134 K (Williams, n.d.), about 135 K (Lindal et al., 1985; Mankovich and Fuller, 2021), or about 143 K (Militzer and Hubbard, 2023).
3. **Galileo probe depth** differs by source: about 132 km below the 1-bar level (Young, 2003), about 150 km (Mousis et al., 2014), and about 180 km or "200 km" on NASA pages (NASA, n.d.-b; NASA, n.d.-c). The differences probably reflect different reference levels; pressure (≈22–23 bar) and duration (≈58 min) agree.
4. **Galileo peak deceleration** is given as 228 g or about 230 g (NASA, n.d.-b).
5. **Cloud-deck pressures** come from equilibrium models with assumed enrichments; a Saturn probe has never measured them.
6. **Saturn conductivity versus depth** has not been measured. The appendix treats σ as a parameter from 0 to 10^4 S/m; the upper value is a model expectation for >10^6 bar (Mankovich and Fuller, 2021; Liu et al., 2014), and no measured value exists for the cloud decks.

15.3 Calculations, extrapolations, and design labels

1. **Terminal velocities, descent profiles, survival windows and N_{live}** are simplified calculations (ESTIMATE) assuming m = 0.1 kg, C_d = 0.5, g ≈ 10 m/s², an isothermal scale height and no wind. The isothermal model overestimates deep band-traversal times, because real temperatures rise with depth.
2. **Node spacing of hundreds of metres to about 1 km** applies to UHF links in the upper troposphere only. Label:
   ORDER-OF-MAGNITUDE DESIGN ESTIMATE, NOT A DERIVED MISSION REQUIREMENT
3. **The 10,000-node tranche, the 0.1 kg node mass and the ≈1 t total** are design choices for discussion.
4. **Link budgets (Appendix A.1)** assume a coil radius of 18 mm, 100 turns, 1 Ω coil resistance, a thermal noise floor at 300 K, 10 Hz bandwidth and SNR = 10. Real Saturn radio noise (for example from lightning) is unknown here and probably higher, which would make the results worse.
5. **Material strengths (Appendix A.4)** are room-temperature manufacturer or laboratory values; elevated temperature, hydrogen exposure, flaws and buckling would lower failure pressures. At megabar pressures a yield-strength comparison is inadequate.
6. **Sr-90 and Cs-137 power values** are my calculations from LNHB decay data; betavoltaic efficiencies (0.2–2%) and source loadings are assumptions.
7. **Entry survival fractions (Appendix A.6)** scale from one published Saturn probe design with an assumed nose radius and an assumed log-normal model scatter; they are illustrative only.
8. **The iterative-descent loop** is an untested research programme. Laboratory synthesis of a high-pressure phase does not imply that a macroscopic, structurally useful shell can be made from it.
9. **Shell staging, swarm economics, band specialisation and the mesh relay** are labelled HYPOTHESIS or UNTESTED throughout.

15.4 Partly verified citations

1. Barr et al. (2000), Sun and Akyildiz (2010), Milos (1997), and Mao et al. (2018): bibliographic metadata verified only; cited for general statements.
2. Olsen et al. (2012) and Zhou et al. (2021): only short abstracts or summaries seen; cited for the general point that betavoltaics are low-power and low-efficiency.
3. Liu et al. (2014): secondary citation as used by Mankovich and Fuller (2021).
4. National Research Council (2009): summary-level, including its description by the World Nuclear Association.
5. Jackson (1999) and Timoshenko and Goodier (1970): standard textbook results; page numbers not re-checked.
6. Fortney et al. (2023): preprint of an accepted book chapter; final pagination not checked.

7. NASA STMD (2026): solicitation details read through a third-party listing reproducing the official notice; the NSPIRES document itself was not opened.
8. Manufacturer datasheets (Goodfellow (n.d.), Heraeus (n.d.), SICT (n.d.)) give indicative values that vary with grade and processing.
9. Several web pages (Idaho National Laboratory (n.d.), European Space Agency (n.d.-a), European Space Agency (n.d.-b), European Space Agency (n.d.-c)) were read through a search index. Undated pages are listed as “n.d.” with the access date.

A Quantitative Analysis: Math, Materials, and Probability

This appendix gives the calculations behind the paper’s quantitative statements. Every input is either cited or labelled as an assumption, and every result is an ESTIMATE unless stated otherwise. The script that produces all values is `analysis/appendix_calc.py`. Constants: $\mu_0 = 1.25663706212 \times 10^{-6}$ N/A^2, $k_B = 1.380649 \times 10^{-23}$ J/K, $N_A = 6.02214076 \times 10^{23}$ mol^{-1}, $e = 1.602176634 \times 10^{-19}$ C (Tiesinga et al., 2021). Shell size: outer radius $r_o = 21.5$ mm (43 mm diameter).

A.1 Node spacing and link range in a conducting medium

Model. Two coaxial coils (radius a, N turns, resistance R_c) separated by $r \gg a$ couple through the near-field of a magnetic dipole. The on-axis dipole field $B = \mu_0 m/(2\pi r^3)$ with $m = N I \pi a^2$ (Jackson, 1999) gives the mutual inductance and, for conjugate-matched coils with weak coupling, the power transfer ratio (derived here from the dipole field; cf. Sun and Akyildiz (2010)):

$$M(r) = \frac{\mu_0 N_t N_r (\pi a_t^2)(\pi a_r^2)}{2\pi r^3} = \frac{\mu_0 \pi N_t N_r a_t^2 a_r^2}{2r^3}, \tag{4}$$

$$\frac{P_r}{P_t} \approx \frac{(\omega M(r))^2}{4 R_t R_r} \cdot e^{-2\frac{r}{\delta}}, \quad \delta = \frac{1}{\sqrt{\pi f \mu_0 \sigma}}. \tag{5}$$

The exponential factor applies the plane-wave skin-depth attenuation (Equation 3) to the near field. This is a common first-order approximation, and it is conservative at low σ, where displacement currents dominate and the true attenuation is smaller. The receiver needs $P_{r,min} = k_B T B \cdot SNR$. **Assumptions:** $a = 18$ mm, $N = 100$, $R_c = 1\ \Omega$, $T = 300$ K, $B = 10$ Hz, SNR = 10, giving $P_{r,min} \approx 4.1 \times 10^{-19}$ W. Saturn’s conductivity versus depth is not measured, so σ is a parameter from 0 (insulating) to 10^4 S/m, the model expectation deeper than about 10^6 bar (Mankovich and Fuller, 2021; Liu et al., 2014); for comparison, shocked fluid hydrogen reaches about 2×10^5 S/m at metallization (Nellis et al., 1996).

Results (Table 4). Even in a perfectly insulating gas at 1 kHz, a 100 m hop needs about 10 kW, 500 m about 150 MW, and 1 km about 10 GW, because the received power falls as r^{-6}. With 1 mW transmitted, the insulating-medium range is about 7 m at 1 kHz and about 1.5 m at 10 Hz. Lowering the frequency helps only when σ is large enough that r/δ matters; raising it improves coupling (P_r grows as f^2) until skin-depth loss takes over. For $\sigma \gtrsim 1$ S/m, hops longer than a few skin depths are impossible at any practical power. For comparison, a UHF far-field link at 400 MHz (Friis equation, antenna efficiency 0.1 each, 10 kHz bandwidth, no gas absorption) needs only about 0.1 µW, 3 µW and 12 µW for 100 m, 500 m and 1 km. Ammonia absorption (Folkner et al., 1998) would add loss that is not modelled here.

f	σ (S/m)	δ	P_t: 100 m	P_t: 500 m	P_t: 1 km
1 kHz	0	∞	9.8×10^3 W	1.5×10^8 W	9.8×10^9 W
1 kHz	10^{-6}	15.9 km	9.9×10^3 W	1.6×10^8 W	1.1×10^{10} W
1 kHz	10^{-3}	503 m	1.5×10^4 W	1.1×10^9 W	5.2×10^{11} W
1 kHz	1	15.9 m	2.8×10^9 W	3×10^{35} W	4×10^{64} W
1 kHz	10^2	1.6 m	4×10^{58} W	$\gg 10^{100}$ W	$\gg 10^{100}$ W
10 Hz	0	∞	9.8×10^7 W	1.5×10^{12} W	9.8×10^{13} W
10 Hz	1	159 m	3.4×10^8 W	8.2×10^{14} W	2.8×10^{19} W
10 Hz	10^2	15.9 m	2.8×10^{13} W	3×10^{39} W	4×10^{68} W
10 Hz	10^4	1.6 m	4×10^{62} W	$\gg 10^{100}$ W	$\gg 10^{100}$ W

Table 4: Transmit power required for a golf-ball MI link (Equation 4, Equation 5) versus gap, frequency and conductivity (ESTIMATE; assumptions in text). Values above about 10^3 W are physically meaningless for a 43 mm node and are shown only to make the scaling visible.

Implication for spacing. For golf-ball nodes, the allowable MI gap at milliwatt power is about 1.5–7 m in insulating gas and shorter where σ is appreciable. The hundreds-of-metres-to-1-km spacing in Section 10 is compatible only with UHF links in the non-conducting upper troposphere. No single "optimal gap" is claimed: the allowable gap is whatever Equation 5 permits for the actual σ, f, power and noise, none of which is measured for Saturn's deep atmosphere.

A.2 Survival window and probability of completing an uplink

Survival window. In the isothermal descent model, density scales with pressure, so $v_t = v_0 (P_0/P)^{1/2}$ and $dz = H\, dP/P$. The time to cross a band from P_1 to P_2 is

$$W = \int_{P_1}^{P_2} \frac{H\,\mathrm{d}P}{P v_t} = \frac{2H}{v_0}\left(\sqrt{\frac{P_2}{P_0}} - \sqrt{\frac{P_1}{P_0}}\right), \tag{6}$$

with H = 59.5 km (Williams, n.d.), v_0 = 120 m/s and P_0 = 1 bar (ESTIMATE). A shell is assumed to remain functional while the node is inside its band, so W is the survival window for that shell. Deeper, the true temperature rises, the density is lower than isothermal, and W shrinks, so the S4 value is an upper bound. As a check of scale, the model gives 3,540 s (59 min) from 1 to 21 bar, similar to Galileo's ≈58 min descent to ≈22 bar at Jupiter (NASA, n.d.-b). The agreement is a coincidence of scale, not a validation, since Galileo descended under a parachute on a different planet.

Ablation. Ablation acts only during hypersonic entry (Appendix A.6). During the subsonic descent modelled here, failure is set by pressure, temperature and chemistry, not by ablation. In this appendix the descent-phase destruction rate is therefore represented statistically.

Probability model. The required transmission time is $T_{tx} = D/R$. **Assumption:** D = 1,600 bit (a 200-byte frame). A node's functional lifetime within its band is modelled as exponential with mean equal to W (a memoryless "race" between random failure and transmission), with the hard constraint $T_{tx} \le W$:

$$P_{\text{uplink}} = \exp\left(-\frac{T_{\text{tx}}}{W}\right) \quad (T_{\text{tx}} \le W), \quad P_{\text{uplink}} = 0 \text{ otherwise}\,. \tag{7}$$

Shell / band	P range (bar)	W (s)	ELF 10 bit/s (T_{tx} = 160 s)	VLF 1 kbit/s (1.6 s)	UHF 10 kbit/s (0.16 s)
S1: NH_3 cloud	1–2	409	0.68	0.996	0.9996
S2: NH_4SH cloud	2.5–5	647	0.78	0.998	0.9998
S3: H_2O cloud	8–21	1,734	0.91	0.999	0.99991
S4: design target	100–1,000	≤ 21,370	≤ 0.993	≤ 0.99993	≤ 0.99999

Table 5: Band survival windows (Equation 6) and probability of completing one 1,600-bit uplink (Equation 7). ESTIMATE ; isothermal descent, exponential lifetime with mean W.

Relay load. Each node must also forward the frames of the nodes below it, so every hop must sustain at least D/Δt = 160 bit/s for Δt = 10 s. A 10 bit/s ELF hop cannot keep pace with that release cadence. It could serve only the deepest one or two hops, with heavy compression or slower releases (ESTIMATE).

A.3 Relay chain reliability

Series model (as specified). If a packet must traverse N links in series, each failing independently with probability p, then

$$P_{\text{end}} = (1-p)^N, \quad P_{\text{end}} \geq 0.5 \Longrightarrow p \leq 1 - 0.5^{1/N} \approx \frac{\ln 2}{N}. \tag{8}$$

For N = 10,000: p = 10^{-3} gives P_{end} = 4.5 × 10^{-5} p = 10^{-4} gives 0.368; p = 10^{-5} gives 0.905; p = 10^{-6} gives 0.990. Keeping P_{end} ≥ 50% requires p ≤ 6.93 × 10^{-5} (Table 6). Because only about N_{live} ≈ 360 nodes are alive at once (Section 6), the instantaneous relay path is far shorter than 10,000 hops. The N = 360 column shows how much that relaxes the requirement.

p (per link)	P_{end}, N = 10,000	P_{end}, N = 360	Skip-link approx., N = 10,000
10^{-3}	4.5 × 10^{-5}	0.698	0.990
10^{-4}	0.368	0.965	0.9999
6.93 × 10^{-5}	0.500	0.975	0.99995
10^{-5}	0.905	0.996	≈1
10^{-6}	0.990	0.9996	≈1

Table 6: End-to-end success of a pure series relay chain (Equation 8), and an approximate skip-link variant. Maximum p for P_{end} ≥ 0.5: 0.067 (N = 10), 6.9 × 10^{-3} (N = 100), 1.9 × 10^{-3} (N = 360), 6.9 × 10^{-4} (N = 1,000), 6.93 × 10^{-5} (N = 10,000).

Redundancy. A pure series chain is brittle. If each node can also reach the node two above (a skip-link), the chain breaks only when two consecutive nodes fail. With independent failures this gives approximately $P_{end} \approx (1 - p^2)^N$, which raises the tolerable p from about 7 × 10^{-5} to about 8 × 10^{-3} for N = 10,000. That improvement depends on the skip-link closing, and Appendix A.1 shows a doubled MI gap is very costly. The skip-link column is therefore an optimistic bound (ESTIMATE).

A.4 Material stress on a golf-ball shell

Model. A spherical shell with outer radius r_o = 21.5 mm and inner radius r_i = 15 mm (6.5 mm wall; assumption) carries an external hydrostatic pressure P with near-zero internal pressure. The Lamé thick-wall solution (Timoshenko and Goodier, 1970) gives the largest compressive hoop stress at the inner surface:

$$\sigma_{\theta,\,\max} = \frac{3Pr_o^3}{2(r_o^3 - r_i^3)} \approx 2.27P. \tag{9}$$

The thin-wall formula σ = P r/(2t) gives 1.40 P at the mid-radius and underestimates the stress for this wall ratio. Failure is taken to occur when $\sigma_{\theta,max}$ reaches the material's room-temperature yield or compressive

strength. Buckling, temperature, hydrogen embrittlement, flaws and joints are not included, and each would lower the failure pressure.

Stress versus depth. At 1, 10, 10^2, 10^3, 10^4, 10^5 and 10^6 atm (1.013×10^5 to 1.013×10^{11} Pa), Equation 9 gives peak stresses of 0.23 MPa, 2.3 MPa, 23 MPa, 230 MPa, 2.3 GPa, 23 GPa and 230 GPa.

Material (source)	Strength (GPa)	Failure P (GPa)	Failure P (atm)
Iridium, annealed–hardened (Heraeus, n.d.)	0.093–1.62 (yield)	0.041–0.71	≈400–7,000
Tungsten, soft–hard (Goodfellow, n.d.)	0.55–1.92 (yield–tensile)	0.24–0.85	≈2,400–8,300
Alumina (SICT, n.d.)	1.7–2.5 (compr.)	0.75–1.10	≈7,400–10,900
Alumina–zirconia composite (SICT, n.d.)	2.0 (compr.)	0.88	≈8,700
Silicon carbide (SICT, n.d.)	2.5–3.9 (compr.)	1.10–1.72	≈10,900–17,000
Diamond (Eremets et al., 2005)	130–140 (yield)	57–62	≈$5.6–6.1 \times 10^5$

Table 7: Failure pressures of a 43 mm shell (6.5 mm wall) under external pressure, from Equation 9 and room-temperature strengths (ESTIMATE). 1 GPa ≈ 9,869 atm. For tungsten, the 1.92 GPa upper value is a hard-wire tensile strength used as a proxy.

Interpretation. Under this model, every metal and engineering ceramic fails at about 400–17,000 atm (≈0.04–1.7 GPa), far above the cloud decks (≤ 21 atm) but within the molecular envelope. A monolithic diamond shell would, on paper, reach about 6×10^5 atm and still fall short of 10^6 atm. No 43 mm monolithic diamond pressure shell has been made, and diamond's behaviour at high temperature in hydrogen is a separate question. At megabar pressures a "yield strength" comparison stops being meaningful: materials transform to high-pressure phases (Section 9) and the relevant question becomes phase stability, not elastic strength. Pressure-compensated (fluid-filled) designs, which reduce the pressure difference across the shell, are a possible alternative but are not analysed here.

A.5 Power budget

Specific activity and power. For a nuclide with half-life $t_{1/2}$ and molar mass M, the specific activity is $A_s = (\ln 2 / t_{1/2})\, N_A/M$, and the specific thermal power is $A_s \bar{E}$, where $\bar{E}$ is the mean energy deposited per decay. Using LNHB data (LNHB, 2005a; LNHB, 2005b; LNHB, n.d.) and mass numbers for M:

- **Sr-90 + Y-90:** $t_{1/2}$ = 28.80 a; $\bar{E}_\beta$ = 196 + 926.7 keV. Result: $A_s = 5.1 \times 10^{12}$ Bq/g and 0.92 W/g, all from beta particles, which are absorbed locally.
- **Cs-137:** $t_{1/2}$ = 30.018 a; beta branches 173.67 keV (94.57%) and 284.90 keV (5.43%), plus about 9.6% conversion electrons near 0.63 MeV. Result: $A_s = 3.2 \times 10^{12}$ Bq/g, with about 0.12 W/g in electrons. The 661.657 keV gamma (85.01%) carries another 0.29 W/g, which mostly escapes a small source and must be shielded. This is the strong-gamma penalty that rules Cs-137 out.

Volume. A 43 mm sphere has a volume of 41.6 cm^3. **Assumptions:** source loadings of 10 mg, 100 mg and 1 g of Sr-90 (the last is about 0.4 cm^3 of a strontium ceramic, about 1% of the volume, before shielding); a betavoltaic total efficiency η = 0.2–2% (Zhou et al., 2021; Olsen, 1993); and encapsulation plus shielding taking a large, unquantified fraction of the node mass.

Sr-90 load	Activity	Heat	Electric (η 0.2–2%)	Duty, 1 mW Tx	Duty, 10 kW Tx
10 mg	5.1×10^{10} Bq (1.4 Ci)	9.2 mW	18–180 µW	1.8–18%	1.8×10^{-9} to 1.8×10^{-8}
100 mg	5.1×10^{11} Bq (14 Ci)	92 mW	0.18–1.8 mW	18–100%	1.8×10^{-8} to 1.8×10^{-7}
1 g	5.1×10^{12} Bq (138 Ci)	0.92 W	1.8–18 mW	100%	1.8×10^{-7} to 1.8×10^{-6}

Table 8: Betavoltaic power and achievable duty cycle $d = P_e/P_{tx}$ (ESTIMATE). The 1 mW transmitter corresponds to a ≈7 m MI hop and 10 kW to a ≈100 m hop in insulating gas at 1 kHz (Appendix A.1).

Interpretation. A golf-ball volume can support a milliwatt-class transmitter at a useful duty cycle, which is enough for the ≈7 m MI hops of Appendix A.1. It cannot support continuous transmission at the power a 100 m–1 km ELF/VLF hop would need (duty cycles of 10^{-6} or less). At 1 g per node, the 10,000-node tranche would carry about 10 kg of Sr-90 (≈5×10^{16} Bq). That raises the regulatory issues of Section 7 sharply and strengthens the case for primary chemical cells over node lifetimes of hours. Spent-fuel plutonium is not considered, for the reasons in Section 7.

A.6 Atmospheric entry heating and survival fraction

Entry conditions. For Saturn, typical inertial entry speeds are about 36 km/s or more. A prograde, near-equatorial entry benefits from Saturn's rotation, reducing the atmosphere-relative speed to about 26 km/s. Studied entry flight-path angles (EFPA) run from −8° to −19° (Mousis et al., 2016). The Hera design (220 kg, ballistic coefficient $\beta = 269$ kg/m^2) needed 23.8–39.3 kg of HEEET thermal protection (mass fraction 0.11–0.18) and saw peak heat fluxes of about 1.2–2.6 kW/cm^2 at 36 km/s inertial and 10° latitude (Mousis et al., 2016).

Scaling. Stagnation-point convective heating follows the Sutton–Graves form $q \propto (\rho/R_n)^{1/2} V^3$ (Carroll and Brandis, 2022). In a ballistic entry, peak heating occurs where ρ scales as $\beta \sin\gamma / H$ (Allen and Eggers, 1958). Hence

$$q_{\max} \propto \sqrt{\frac{\beta \sin\gamma}{R_n}} V_E^3, \quad Q \propto \sqrt{\frac{\beta}{R_n \sin\gamma}} V_E^2, \tag{10}$$

where Q is the integrated heat load. Thermal-protection mass fraction is taken to scale with Q (an assumption), calibrated to Hera at EFPA −19° (f = 0.108) with an **assumed** Hera nose radius $R_n = 0.25$ m.

Bare node. A bare node has m = 0.1 kg, an assumed hypersonic $C_d = 0.92$ and $A = 1.45 \times 10^{-3}$ m^2, giving $\beta \approx 75$ kg/m^2 and $R_n = 21.5$ mm. Equation 10 then gives a peak heat flux of about 2.2–4.7 kW/cm^2 (about 1.8 × Hera's) and a required ablator fraction of about 0.30 (−8°), 0.23 (−14°) and 0.19 (−19°).

Survival fraction. Each node has an available ablator fraction f_{av}. Delivery dispersion is modelled by drawing γ from a normal distribution with mean γ_0 and standard deviation 1°, and model uncertainty as a log-normal scatter of $\sigma_{ln} = 0.3$ on the required fraction (both assumptions). A node survives entry heating if its required fraction does not exceed f_{av}. A 20,000-sample Monte Carlo gives Table 9.

β (kg/m²)	EFPA γ_0	Required f (median)	f_{av} = 0.1	f_{av} = 0.2	f_{av} = 0.3
25	−8°	0.17	0.04	0.68	0.96
25	−14°	0.13	0.19	0.92	0.997
25	−19°	0.11	0.35	0.97	0.999
75	−8°	0.30	≈0	0.09	0.49
75	−14°	0.23	0.003	0.34	0.83
75	−19°	0.19	0.01	0.53	0.93
200	−8°	0.49	0	0.002	0.06
200	−14°	0.37	0	0.02	0.25
200	−19°	0.32	0	0.06	0.42

Table 9: Fraction of bare nodes surviving entry heating versus ballistic coefficient, EFPA and available ablator fraction (ESTIMATE ; scaled from Mousis et al. (2016) with Equation 10, assumed nose radius, dispersion and model scatter). β = 75 kg/m² is the 0.1 kg, 43 mm node; β = 25 kg/m² would require a 33 g node.

Interpretation. A bare 0.1 kg node would need roughly a quarter to a third of its mass as ablator to have good odds of surviving entry, at heat fluxes above those of the studied Saturn probe. This supports the baseline in Section 5: carry all nodes inside a shared aeroshell, so that node survival through entry equals aeroshell survival, for which flown heritage exists. These fractions ignore radiative heating, shape change and mechanical loads, and they rest on an assumed reference nose radius. They are scaling estimates only, not a thermal-protection design.

References

Akahama, Y., Kawamura, H., Häusermann, D., Hanfland, M., Shimomura, O., 1995. New high-pressure structural transition of oxygen at 96 GPa associated with metallization in a molecular solid. Phys. Rev. Lett. 74, 4690–4693. https://doi.org/10.1103/PhysRevLett.74.4690

Allen, H.J., Eggers, A.J., Jr., 1958. A study of the motion and aerodynamic heating of ballistic missiles entering the earth's atmosphere at high supersonic speeds. NACA Report 1381. https://ntrs.nasa.gov/citations/19930091020

Barr, R., Jones, D.L., Rodger, C.J., 2000. ELF and VLF radio waves. J. Atmos. Sol.-Terr. Phys. 62, 1689–1718. https://doi.org/10.1016/S1364-6826(00)00121-8

Bolton, S.J., Adriani, A., Adumitroaie, V., Allison, M., Anderson, J., Atreya, S., et al., 2017. Jupiter's interior and deep atmosphere: The initial pole-to-pole passes with the Juno spacecraft. Science 356, 821–825. https://doi.org/10.1126/science.aal2108

Brygoo, S., Loubeyre, P., Millot, M., Rygg, J.R., Celliers, P.M., Eggert, J.H., Jeanloz, R., Collins, G.W., 2021. Evidence of hydrogen–helium immiscibility at Jupiter-interior conditions. Nature 593, 517–521. https://doi.org/10.1038/s41586-021-03516-0

Carroll, A.T., Brandis, A.M., 2022. Stagnation point convective heating correlations for entry into H2/He atmospheres. AIAA Aviation 2022 Forum (NASA NTRS 20220018610). https://ntrs.nasa.gov/citations/20220018610

Celliers, P.M., Millot, M., Brygoo, S., McWilliams, R.S., Fratanduono, D.E., Rygg, J.R., et al., 2018. Insulator-metal transition in dense fluid deuterium. Science 361, 677–682. https://doi.org/10.1126/science.aat0970

Defense Advanced Research Projects Agency, n.d. Defense Sciences Office. DARPA web page, accessed November 2026. https://www.darpa.mil/about/offices/dso

Del Genio, A.D., Achterberg, R.K., Baines, K.H., Flasar, F.M., Read, P.L., Sánchez-Lavega, A., Showman, A.P., 2009. Saturn atmospheric structure and dynamics. In: Dougherty, M.K., Esposito, L.W., Krimigis, S.M. (Eds.), Saturn from Cassini-Huygens. Springer, Dordrecht, pp. 113–159. https://doi.org/10.1007/978-1-4020-9217-6_6

Desgreniers, S., Vohra, Y.K., Ruoff, A.L., 1990. Optical response of very high density solid oxygen to 132 GPa. J. Phys. Chem. 94, 1117–1122. https://doi.org/10.1021/j100366a020

Dong, X., Oganov, A.R., Goncharov, A.F., Stavrou, E., Lobanov, S., Saleh, G., et al., 2017. A stable compound of helium and sodium at high pressure. Nat. Chem. 9, 440–445. https://doi.org/10.1038/nchem.2716

Dubrovinsky, L., Dubrovinskaia, N., Prakapenka, V.B., Abakumov, A.M., 2012. Implementation of micro-ball nanodiamond anvils for high-pressure studies above 6 Mbar. Nat. Commun. 3, 1163. https://doi.org/10.1038/ncomms2160

Duffy, T.S., Smith, R.F., 2019. Ultra-high pressure dynamic compression of geological materials. Front. Earth Sci. 7, 23. https://doi.org/10.3389/feart.2019.00023

Eremets, M.I., Trojan, I.A., Gwaze, P., Huth, J., Boehler, R., Blank, V.D., 2005. The strength of diamond. Appl. Phys. Lett. 87, 141902. https://doi.org/10.1063/1.2061853

European Space Agency, n.d.-a. Funding your ideas (OSIP). ESA Space Technology web page, accessed November 2026. https://technology.esa.int/page/funding-your-ideas

European Space Agency, n.d.-b. The Open Space Innovation Platform (OSIP). ESA web article, accessed November 2026. https://www.esa.int/ga/articles/the-open-space-innovation-platform-osip

European Space Agency, n.d.-c. ESA opening up to new ideas. ESA Space Engineering & Technology web article, accessed November 2026. https://www.esa.int/Enabling_Support/Space_Engineering_Technology/ESA_opening_up_to_new_ideas

Folkner, W.M., Woo, R., Nandi, S., 1998. Ammonia abundance in Jupiter's atmosphere derived from the attenuation of the Galileo probe's radio signal. J. Geophys. Res. 103, 22847–22855. https://doi.org/10.1029/98JE01635

Fortney, J.J., Militzer, B., Mankovich, C.R., Helled, R., Wahl, S.M., Nettelmann, N., Hubbard, W.B., Stevenson, D.J., Iess, L., Marley, M.S., Movshovitz, N., 2023. Saturn's interior after the Cassini Grand Finale. Preprint, arXiv:2304.09215; chapter accepted for Baines, K.H., et al. (Eds.), Saturn: The Grand Finale. Cambridge University Press. https://arxiv.org/abs/2304.09215

Goodfellow, n.d. Tungsten straight wire (99.95%): material properties data sheet. Manufacturer data, accessed November 2026. https://www.goodfellow.com/usa/technical_data/pdf/download?sku=1000005861-group

Heraeus Precious Metals, n.d. Iridium datasheet. Manufacturer data, accessed November 2026. https://pim.heraeus.com/datasheets/HPM/FM/Contact%20Materials/Iridium_Datasheet_EN_(Heraeus_Precious_Metals).pdf

Idaho National Laboratory, n.d. National labs resume plutonium production for space exploration. Web article, accessed November 2026. https://inl.gov/national-labs-resume-plutonium-production-for-space-exploration/

Iess, L., Militzer, B., Kaspi, Y., Nicholson, P., Durante, D., Racioppa, P., et al., 2019. Measurement and implications of Saturn's gravity field and ring mass. Science 364, eaat2965. https://doi.org/10.1126/science.aat2965

Jackson, J.D., 1999. Classical Electrodynamics, third ed. Wiley, New York. ISBN 978-0-471-30932-1

Knudson, M.D., Desjarlais, M.P., Becker, A., Lemke, R.W., Cochrane, K.R., Savage, M.E., Bliss, D.E., Mattsson, T.R., Redmer, R., 2015. Direct observation of an abrupt insulator-to-metal transition in dense liquid deuterium. Science 348, 1455–1460. https://doi.org/10.1126/science.aaa7471

Laboratoire National Henri Becquerel (LNE–LNHB/CEA), 2005a. Table de radionucléides: Sr-90 (V. Chisté). Recommended decay data. https://www.lnhb.fr/nuclides/Sr-90_tables.pdf

Laboratoire National Henri Becquerel (LNE–LNHB/CEA), 2005b (revised 2015). Table de radionucléides: Y-90. Recommended decay data. https://www.lnhb.fr/nuclides/Y-90_tables.pdf

Laboratoire National Henri Becquerel (LNE–LNHB/CEA), n.d. Table de radionucléides: Cs-137. Recommended decay data. https://www.lnhb.fr/nuclides/Cs-137_tables.pdf

Lindal, G.F., Sweetnam, D.N., Eshleman, V.R., 1985. The atmosphere of Saturn: An analysis of the Voyager radio occultation measurements. Astron. J. 90, 1136. https://doi.org/10.1086/113820

Liu, J., Schneider, T., Fletcher, L.N., 2014. Constraining the depth of Saturn's zonal winds by measuring thermal and gravitational signals. Icarus 239, 260–272. https://doi.org/10.1016/j.icarus.2014.05.036

Ma, Y., Eremets, M., Oganov, A.R., Xie, Y., Trojan, I., Medvedev, S., Lyakhov, A.O., Valle, M., Prakapenka, V., 2009. Transparent dense sodium. Nature 458, 182–185. https://doi.org/10.1038/nature07786

Mankovich, C.R., Fuller, J., 2021. A diffuse core in Saturn revealed by ring seismology. Nat. Astron. 5, 1103–1109. https://doi.org/10.1038/s41550-021-01448-3

Mao, H.-K., Chen, X.-J., Ding, Y., Li, B., Wang, L., 2018. Solids, liquids, and gases under high pressure. Rev. Mod. Phys. 90, 015007. https://doi.org/10.1103/RevModPhys.90.015007

Matsuoka, T., Shimizu, K., 2009. Direct observation of a pressure-induced metal-to-semiconductor transition in lithium. Nature 458, 186–189. https://doi.org/10.1038/nature07827

Militzer, B., Hubbard, W.B., 2023. Relation of gravity, winds, and the moment of inertia of Jupiter and Saturn. Planet. Sci. J. 4, 95. https://doi.org/10.3847/PSJ/acd2cd

Militzer, B., Wahl, S., Hubbard, W.B., 2019. Models of Saturn's interior constructed with an accelerated concentric Maclaurin spheroid method. Astrophys. J. 879, 78. https://doi.org/10.3847/1538-4357/ab23f0

Milos, F.S., 1997. Galileo probe heat shield ablation experiment. J. Spacecr. Rockets 34, 705–713. https://doi.org/10.2514/2.3293

Morales, M.A., Schwegler, E., Ceperley, D., Pierleoni, C., Hamel, S., Caspersen, K., 2009. Phase separation in hydrogen–helium mixtures at Mbar pressures. Proc. Natl. Acad. Sci. U.S.A. 106, 1324–1329. https://doi.org/10.1073/pnas.0812581106

Mousis, O., Atkinson, D.H., Spilker, T., Venkatapathy, E., Poncy, J., Frampton, R., Coustenis, A., Reh, K., et al., 2016. The Hera Saturn entry probe mission. Planet. Space Sci. 130, 80–103. https://doi.org/10.1016/j.pss.2015.06.020

Mousis, O., Fletcher, L.N., Lebreton, J.-P., Wurz, P., Cavalié, T., Coustenis, A., et al., 2014. Scientific rationale for Saturn's in situ exploration. Planet. Space Sci. 104, 29–47. https://doi.org/10.1016/j.pss.2014.09.014

NASA Radioisotope Power Systems Program, n.d.-d. About plutonium-238. Web page, accessed November 2026. https://science.nasa.gov/planetary-science/programs/radioisotope-power-systems/about-plutonium-238/

NASA Space Technology Mission Directorate, 2026. NASA Innovative Advanced Concepts (NIAC) Phase I, Appendix NNH26ZTR001N-27NIAC_A1 to SpaceTech-REDDI-2026. Solicitation summary as listed on Grants.gov aggregators, posted 28 September 2026. https://grantround.com/grants/nnh26ztr001n-27niac-a1

NASA, n.d.-a. Cassini Grand Finale. NASA Science web page, accessed November 2026. https://science.nasa.gov/mission/cassini/grand-finale/

NASA, n.d.-b. Galileo Jupiter atmospheric probe. NASA Science web page, accessed November 2026. https://science.nasa.gov/mission/galileo-jupiter-atmospheric-probe/

NASA, n.d.-c. Galileo: Science. NASA Science web page, accessed November 2026. https://science.nasa.gov/mission/galileo/galileo-science/

NASA, n.d.-e. Apply to NIAC (NASA Innovative Advanced Concepts). NASA web page, accessed November 2026. https://www.nasa.gov/work-with-us/

National Research Council, 2009. Radioisotope Power Systems: An Imperative for Maintaining U.S. Leadership in Space Exploration. The National Academies Press, Washington, DC. https://doi.org/10.17226/12653

Nellis, W.J., Weir, S.T., Mitchell, A.C., 1996. Metallization and electrical conductivity of hydrogen in Jupiter. Science 273, 936–938. https://doi.org/10.1126/science.273.5277.936

Olsen, L.C., 1993. Review of betavoltaic energy conversion. NASA Conference Publication (NTRS 19940006935). https://ntrs.nasa.gov/citations/19940006935

Olsen, L.C., Cabauy, P., Elkind, B.J., 2012. Betavoltaic power sources. Phys. Today 65 (12), 35–38. https://doi.org/10.1063/PT.3.1820

SICT (Société Industrielle de Céramiques Techniques), n.d. Compressive strength: comparative table of mechanical properties of technical ceramics. Manufacturer data, accessed November 2026. https://ceramique-technique.com/en/properties/compressive-strength

Schöttler, M., Redmer, R., 2018. Ab initio calculation of the miscibility diagram for hydrogen–helium mixtures. Phys. Rev. Lett. 120, 115703. https://doi.org/10.1103/PhysRevLett.120.115703

Shimizu, K., Suhara, K., Ikumo, M., Eremets, M.I., Amaya, K., 1998. Superconductivity in oxygen. Nature 393, 767–769. https://doi.org/10.1038/31656

Stevenson, D.J., 2020. Jupiter's interior as revealed by Juno. Annu. Rev. Earth Planet. Sci. 48, 465–489. https://doi.org/10.1146/annurev-earth-081619-052855

Stevenson, D.J., Salpeter, E.E., 1977. The phase diagram and transport properties for hydrogen-helium fluid planets. Astrophys. J. Suppl. Ser. 35, 221. https://doi.org/10.1086/190478

Sun, Z., Akyildiz, I.F., 2010. Magnetic induction communications for wireless underground sensor networks. IEEE Trans. Antennas Propag. 58, 2426–2435. https://doi.org/10.1109/TAP.2010.2048858

The White House, 2019. Presidential Memorandum on Launch of Spacecraft Containing Space Nuclear Systems (National Security Presidential Memorandum-20), 20 August 2019. Daily Compilation of Presidential Documents DCPD-201900558. https://www.govinfo.gov/content/pkg/DCPD-201900558/pdf/DCPD-201900558.pdf

Tiesinga, E., Mohr, P.J., Newell, D.B., Taylor, B.N., 2021. CODATA recommended values of the fundamental physical constants: 2018. Rev. Mod. Phys. 93, 025010. https://doi.org/10.1103/RevModPhys.93.025010

Timoshenko, S.P., Goodier, J.N., 1970. Theory of Elasticity, third ed. McGraw-Hill, New York. ISBN 978-0-07-064720-6

U.S. Environmental Protection Agency, n.d.-a. Radionuclide basics: Cesium-137. Web page, accessed November 2026. https://www.epa.gov/radiation/radionuclide-basics-cesium-137

U.S. Environmental Protection Agency, n.d.-b. Radionuclide basics: Strontium-90. Web page, accessed November 2026. https://www.epa.gov/radiation/radionuclide-basics-strontium-90

United Nations General Assembly, 1992. Principles Relevant to the Use of Nuclear Power Sources in Outer Space. Resolution A/RES/47/68. https://www.unoosa.org/oosa/en/ourwork/spacelaw/principles/nps-principles.html

Wahl, S.M., Hubbard, W.B., Militzer, B., Guillot, T., Miguel, Y., Movshovitz, N., et al., 2017. Comparing Jupiter interior structure models to Juno gravity measurements and the role of a dilute core. Geophys. Res. Lett. 44, 4649–4659. https://doi.org/10.1002/2017GL073160

Weidenschilling, S.J., Lewis, J.S., 1973. Atmospheric and cloud structures of the Jovian planets. Icarus 20, 465–476. https://doi.org/10.1016/0019-1035(73)90019-5

Williams, D.R., n.d. Saturn Fact Sheet. NASA Space Science Data Coordinated Archive, accessed November 2026. https://nssdc.gsfc.nasa.gov/planetary/factsheet/saturnfact.html

World Nuclear Association, n.d. Plutonium. Information Library, accessed November 2026. https://world-nuclear.org/information-library/nuclear-fuel-cycle/fuel-recycling/plutonium

Young, R.E., 1998. The Galileo probe mission to Jupiter: Science overview. J. Geophys. Res. 103, 22775–22790. https://doi.org/10.1029/98JE01051

Young, R.E., 2003. The Galileo probe: How it has changed our understanding of Jupiter. NASA Technical Reports Server, document 20030053065. https://ntrs.nasa.gov/citations/20030053065

Zhou, C., Zhang, J., Wang, X., Yang, Y., Xu, P., Li, P., Zhang, L., Chen, Z., Feng, H., Wu, W., 2021. Review—Betavoltaic cell: The past, present, and future. ECS J. Solid State Sci. Technol. 10, 027005. https://doi.org/10.1149/2162-8777/abe423